

## **3. Experimental**



### **3. EXPERIMENTAL**

As it has been discussed in the Introduction of this work, the study of SnO<sub>2</sub> as gas sensing material is motivated because of its intrinsic physicochemical properties but also due to its low-cost when compared with actual materials. In this context, the actual efforts are directed to increase the sensibility, selectivity, speed of response and stability of these materials without changing very much the final cost of the device. One of the most important factors affecting these properties is the presence of metals at low concentrations on SnO<sub>2</sub>. Thus, different metals promote better responses to different gases and the chemical state of the metals, together with their dispersion on the SnO<sub>2</sub> surface are very important for gas-sensing properties.

This part of the work deals with the description of the different experimental procedures used, including the new metal addition method that has been developed. Thus, at the first stages of this work, the main aim was to develop an addition method that can fulfil as much as possible of the different requirements needed, that can be summarised as follows: - the developed method must be of low cost, reproducible and as simple as possible; - it must give a fine dispersion of metals on the SnO<sub>2</sub> surface; - contamination from the used chemical reagents should be avoided. Actual methods of addition of metals, that have been briefly described in the Introduction section, are not good enough either because of their cost, because they are difficult to implement in industrial processes or because they give a poor dispersion of the metal on the substrate surface. This last one is the main drawback of impregnation, that actually is the most extended metal addition method mainly because of its simplicity and low cost, but that gives a poor dispersion of the metal when using a one-step process because it basically consists on the evaporation of an aqueous solution of the metal, thereby precipitating the metal salt by supersaturation of the solution. The metal salt remains on the substrate surface by means of van der Waals forces. Impregnation does not allow to control the metal chemical state as, without annealing, the oxidation state is that of the metal salt used as precursor.

When trying to develop a new method, several uncertainties are always present at the beginning of the work and, thus, several possibilities must be explored before the final chose is made. It is at this stage of a certain project where the interactions that the researcher has had with researchers of other fields can be very important as, for example, some methods widely known in certain fields of science can be applied to other fields with only slight modifications, and it is possible that it has not been the case because of the absence of these interactions. Thus, from the preliminary studies performed, the electroless addition of metals using Sn(II) as reductor was chosen as the one to be studied because it fulfilled several of the requirements mentioned above. Thus, the method is of low cost, as all the chemical reagents required are not expensive (except, of course, metal salts, but these reagents are common to any addition method), and electroless metal deposition are reproducible and quite simple methods, that have been studied since 1946 [125]. Moreover, the different chemical reagents used do not contaminate the final material when a proper annealing is performed. Thus, both chlorides and sulphates and ammonium cations are eliminated when annealing at sufficiently high temperatures and, moreover, either Sn(II) or Sn(IV) species coming from the used reductor also give SnO<sub>2</sub> when annealed in air at sufficiently high temperature. The use of SnO<sub>2</sub> nanopowders as base material also facilitates the growth of SnO<sub>2</sub> coming from the reductor, but there were no certainties concerning the final dispersion of the metal on the SnO<sub>2</sub> surface. With respect to

this, only the bibliography of the electroless deposition of Pd using Sn(II) as reductor was present [163-167]. Nevertheless, this is used only as a preliminary step for the deposition of other metals and, thus, no studies of Pd electroless deposition were present at the beginning of this work. Moreover, there were no data available referring the Pd dispersion using SnO<sub>2</sub> as substrate in the electroless method. Thereby, we only had the data concerning other addition methods and/or other substrates, and both of them can change the metal dispersion features. Nevertheless, the fact (stated at the beginning of the study) that the electroless reaction with Sn(II) takes place mainly in solution, and thereby that it was not greatly influenced by the substrate, together with the ‘chemical intuition’ of the author were enough to begin the study of this method as a possible alternative to existing methods.

Thus, now that the scientific background used for the development of the electroless metal addition method has been explained, let discuss the different experimental methods used.

### **3.1. Metal addition methods on tin oxide**

In this section, we will describe the different experimental procedures used for the addition of the different catalysts along this work. First, we will present the impregnation method used for the sake of comparison, thereby presenting the electroless method, and finishing with the addition processes used for other metals (Ru and Ni).

#### **3.1.1. Description of the impregnation method used in this work**

There is a lot of research about the impregnation method but, as the aim of this work was only the comparison with the electroless method, all the impregnation parameters were fixed to be as much comparable as possible with the ones used in the electroless method.

##### **3.1.1.1. Impregnation with palladium**

Typically, 2 gr. of SnO<sub>2</sub> nanopowders were added to 100 cm<sup>3</sup> of a PdCl<sub>2</sub> aqueous solution of the desired concentration, with HCl (5·10<sup>-3</sup> M). The solution was rinsed in a Memmert model WB14 bath provided with a M00 rinsing machine, thus obtaining a solid suspension of the SnO<sub>2</sub> powder in the catalyst solution. The temperature (30 °C) and the rinse rate were maintained during 50 minutes. From this point, two different processes were applied: a) Filtration using Albet model 420 filters is released, rinsing with diluted HCl and then with water. These filters were tried because their pore size is small enough to retain the wet SnO<sub>2</sub> powders but big enough to have a fast filtration time. A final desiccation process at 80 °C was done to collect the final powder; b) The temperature was progressively increased until it reached 80 °C, where it was maintained (still rinsing) until the complete evaporation of the solution, when the dried powders were collected. These two processes were applied to study the influence of the evaporation process on the final additive percentage.

We have used two different nominal atomic Pd/Sn ratios: 1% and 5% in atomic concentration. These ratios were tried to have a direct comparison with the samples prepared with the electroless process.

Then, a thermal treatment is applied on some of the obtained powders using a muffle furnace. This treatment consists of an 8 hours heating in air at the desired temperature (either 450 or 800 °C), reached at a rate of 20 °C min<sup>-1</sup>

### **3.1.1.2. Impregnation with platinum**

2 gr. of SnO<sub>2</sub> nanopowders were added to 100 cm<sup>3</sup> of a (NH<sub>4</sub>)<sub>2</sub>PtCl<sub>4</sub> aqueous solution of the desired concentration in 2.5·10<sup>-3</sup> M H<sub>2</sub>SO<sub>4</sub>. The solution was rinsed in a Memmert model WB14 bath provided with a M00 rinsing machine, thus obtaining a solid suspension of the SnO<sub>2</sub> powder in the catalyst solution. The temperature (30 °C) and the rinse rate were maintained during 1 hour. From this point, two different processes were applied: a) Filtration using Albet model 420 filters is released, rinsing with diluted H<sub>2</sub>SO<sub>4</sub> and then with water. A final desiccation process at 80 °C was done to collect the final powder; b) The temperature was progressively increased until it reached 80 °C, where it was maintained (still rinsing) until the complete evaporation of the solution, when the dried powders were collected. These two processes were applied to study the influence of the evaporation process on the final additive percentage.

We have used two different nominal atomic Pt/Sn ratios: 2% and 10% in atomic concentration. These ratios were tried to have a direct comparison with the samples prepared with the electroless process.

Then, a thermal treatment is applied on some of the obtained powders using a muffle furnace. This treatment consists of an 8 hours heating in air at the desired temperature (either 450 or 800 °C), reached at a rate of 20 °C min<sup>-1</sup>

## **3.1.2. Description of the electroless procedures used in this work**

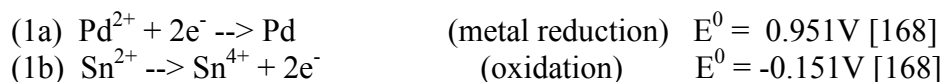
### **3.1.2.1. Pd using Sn(II) as reductor**

The preparation of catalysed tin oxide has been made adding 2 gr of an SnO<sub>2</sub> powder to 100 cm<sup>3</sup> of a PdCl<sub>2</sub> aqueous solution with the corresponding palladium concentration in 5·10<sup>-3</sup> M in HCl (since acid enables the palladium salt solution process, we choose the proposed solution to have anytime an excess of the acid with respect to the different palladium concentrations studied). The solution is then rinsed at the same rate than in the impregnation process, thus obtaining a solid suspension of the SnO<sub>2</sub> powder in the catalyst solution. The temperature (30 °C) and the rinse rate were maintained during 15 minutes just to achieve the thermal equilibrium. Then, 10 cm<sup>3</sup> of a freshly prepared aqueous solution of SnCl<sub>2</sub> in 5·10<sup>-3</sup> M HCl is added and the whole solution is rinsed at the same temperature and rate during 50 minutes.

The basic electroless process is thus as follows:



which can be decomposed into the following half-cell processes:



We have used three different nominal atomic Pd/Sn ratios: 0.1%, 1% and 5% in atomic concentration. These ratios were tried to study the whole range of the usual concentrations used for gas sensing applications of Pd addition on SnO<sub>2</sub> [74]. For each Pd/Sn ratio, two different concentrations of SnCl<sub>2</sub> in the final solution are used: either stoichiometric concentration Sn<sup>2+</sup>/Pd<sup>2+</sup> ratio or 10 times this ratio. Afterwards, a filtration using Albet model 420 filters is released, rinsing with diluted HCl and then with water. A final desiccation process at 80 °C was done to collect the final powder.

Then, a thermal treatment is applied on some of the obtained powders using a muffle furnace. This treatment consists of a 8 hours heating in air at the desired temperature (either 200, 450 or 800 °C), reached at a rate of 20 °C min<sup>-1</sup>

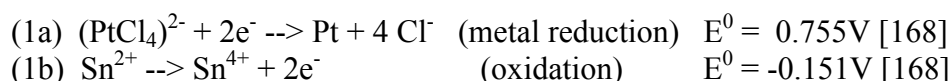
### 3.1.2.2. Pt using Sn(II) as reductor

The preparation of catalysed tin oxide has been made adding 2 gr. of an SnO<sub>2</sub> powder to 100 cm<sup>3</sup> of a (NH<sub>4</sub>)<sub>2</sub>PtCl<sub>4</sub> aqueous solution with the corresponding platinum concentration. The solution is then rinsed at the same rate than in the impregnation process, thus obtaining a solid suspension of the SnO<sub>2</sub> powder in the catalyst solution. The temperature (30 °C) and the rinse rate were maintained during 15 minutes just to achieve the thermal equilibrium. Then, 10 cm<sup>3</sup> of a freshly prepared aqueous solution of SnSO<sub>4</sub> in 2.5·10<sup>-2</sup> M H<sub>2</sub>SO<sub>4</sub> is added and the whole solution is rinsed at the same temperature and rate during 50 minutes. In this case, the addition of the acid facilitates the Sn(II) dissolution and the used acid concentration was chosen in order to have a similar pH in comparison with palladium electroless studies. The change of the anion (chloride in the case of palladium and sulphate here) is due to the occurrence of a competitive process with that of electroless addition of platinum in chloride solutions. This competitive process, basically consisting in a precipitation process, has not been studied yet in detail, but it should be due either to the precipitation of PtCl<sub>2</sub> (only soluble in concentrated HCl) or to the formation of some Pt-Sn complex in the solution, as has been observed elsewhere [169,170] by mixing SnCl<sub>2</sub> and platinum (II) chloride.

The basic electroless process is thus as follows:



which can be decomposed into the following half-cell processes:



We have used three different nominal atomic Pt/Sn ratios: 0.2%, 2% and 10% in atomic concentration. These ratios were tried to study the whole range of the usual concentrations used for gas sensing applications of Pt addition on SnO<sub>2</sub> [171]. For each Pt/Sn ratio, two different concentrations of SnSO<sub>4</sub> in the final solution are used: either the stoichiometric concentration Pt<sup>2+</sup>/Sn<sup>2+</sup> ratio or 10 times this ratio. Afterwards, a filtration using Albet model 420 filters is released, rinsing with diluted H<sub>2</sub>SO<sub>4</sub> and then with water. A final desiccation process at 80 °C was done to collect the final powder.

Then, a thermal treatment is applied on some of the obtained powders using a muffle furnace. This treatment consists of a 8 hours heating in air at the desired temperature (either 200, 450 or 800 °C), reached with a rate of 20 °C min<sup>-1</sup>

### **3.1.3. Addition of Ru and Ni**

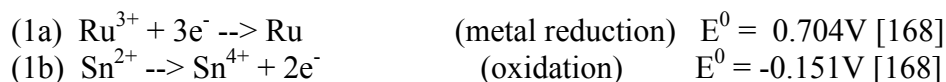
#### **3.1.3.1. Ru addition using Sn(II) chloride**

In this case, a wet impregnation process using Ru and Sn(II) chlorides is usually performed as addition method [172], although the samples undergo a reduction treatment after the catalyst addition to give metallic Ru. In order to have a similar procedure than with the previous catalysts, the preparation of Ru-catalysed tin oxide in our case has been made adding 2 gr. of an SnO<sub>2</sub> powder to 100 cm<sup>3</sup> of a K<sub>2</sub>RuCl<sub>5</sub>·H<sub>2</sub>O aqueous solution 5·10<sup>-3</sup> M in HCl (the acid concentration tried again to have a similar pH than with the other additives). The solution is then rinsed as in previous methods, thus obtaining a solid suspension of the SnO<sub>2</sub> powder in the catalyst solution. The temperature (30 °C) and the rinse rate were maintained during 15 minutes just to achieve the thermal equilibrium. Then, 10 cm<sup>3</sup> of a freshly prepared aqueous solution of SnCl<sub>2</sub> in 5·10<sup>-3</sup> M HCl is added and the whole solution is rinsed at the same temperature and rate during 50 minutes.

The electroless process would be as follows:



which can be decomposed into the following half-cell processes:



We have used three different nominal atomic Ru/Sn ratios: 0.2%, 2% and 10% in atomic concentration. These ratios were tried to have a direct comparison with other additives, like Pt and Ni. For each Ru/Sn ratio, two different concentrations of SnCl<sub>2</sub> in the final solution are used: either stoichiometric concentration Sn<sup>2+</sup>/Ru<sup>3+</sup> ratio or 10 times this ratio. Afterwards, a filtration using Albet model 420 filters is released, rinsing with diluted HCl and then with water. A final desiccation process at 80 °C was done to collect the final powder.

Then, a thermal treatment is applied on some of the obtained powders using a muffle furnace. This treatment consists of an 8 hours heating in air at the desired temperature (either 450 or 800 °C), reached at a rate of 20 °C min<sup>-1</sup>

#### **3.1.3.2. Ni using hypophosphide as reductor**

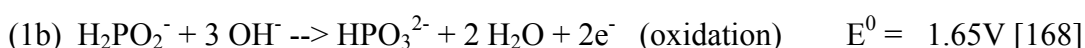
As Sn(II) has not enough reduction power to reduce Ni(II), in this case the preparation of catalysed tin oxide has been using the classical electroless process with hypophosphide. It was typically made adding 2 gr. of a SnO<sub>2</sub> powder to 100 cm<sup>3</sup> of a NiCl<sub>2</sub>·6H<sub>2</sub>O aqueous solution in 0.5 M NH<sub>4</sub>OH. In this case, the pH has to be basic because it is in basic media that the reducing agent is efficient. Thereby, the high concentration of NH<sub>4</sub>OH is needed to reach a basic pH but also to act as Ni(II) complexing agent, in order to prevent the hydroxide precipitation. The solution is then rinsed as previously, thus

obtaining a solid suspension of the SnO<sub>2</sub> powder in the catalyst solution. The temperature (80 °C) and the rinse rate were maintained during 15 minutes just to achieve the thermal equilibrium. Then, 10 cm<sup>3</sup> of a freshly prepared aqueous solution of Na<sub>2</sub>HPO<sub>2</sub> is added and the whole solution is rinsed at the same temperature and rate during 50 minutes.

The basic electroless process is thus as follows:



which can be decomposed into the following half-cell processes:



We have used three different nominal atomic Ni/Sn ratios: 0.2%, 2% and 10% in atomic concentration. These ratios were tried to have a direct comparison with the previous additives. For each Ni/Sn ratio, two different concentrations of reductor in the final solution are used: either the stoichiometric concentration Ni<sup>2+</sup>/H<sub>2</sub>PO<sub>2</sub><sup>-</sup> ratio or 10 times this ratio. Afterwards, a filtration using Albet model 420 filters is released, rinsing with diluted NH<sub>4</sub>OH and then with water. A final desiccation process at 80 °C was done to collect the final powder.

Then, a thermal treatment is applied on some of the obtained powders using a muffle furnace. This treatment consists of a 8 hours heating in air at the desired temperature (either 450 or 800 °C), reached with a rate of 20 °C min<sup>-1</sup>

## **3.2. Tin electrochemical oxidation experiments**

In this section, we will describe the experimental procedure used for the electrochemical experiments described in this work.

### **3.2.1. Preparation of tin polycrystal**

Polycrystalline tin samples had a purity of 99.999% (Goodfellow) and were cut in circles with 10 mm of diameter and 1 mm of width. Prior to the electrochemical measurements, polycrystalline tin was mechanically polished using an alumina paper with a grain size of 3 μm in order to have a proper roughness of the surface. Thus, fig. 3.1 shows an image of the samples as received from the provider. A typical surface after the polishing process is imaged in fig. 3.2.

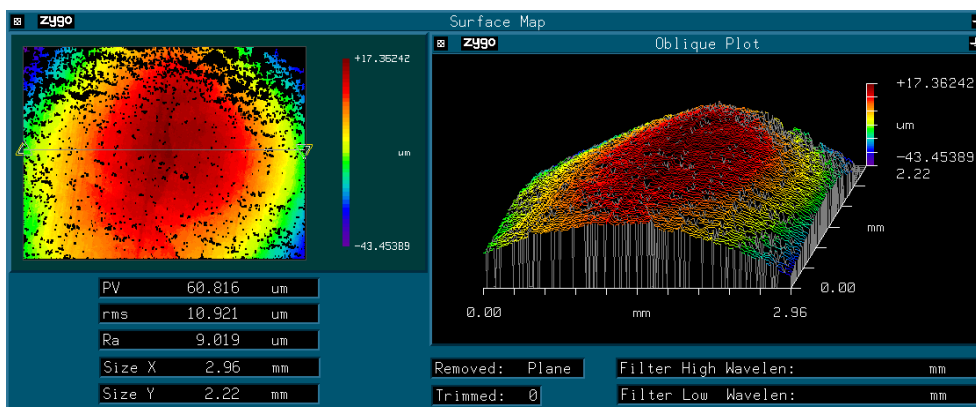


**Fig. 3.1.** Tin polycrystal surface as received.

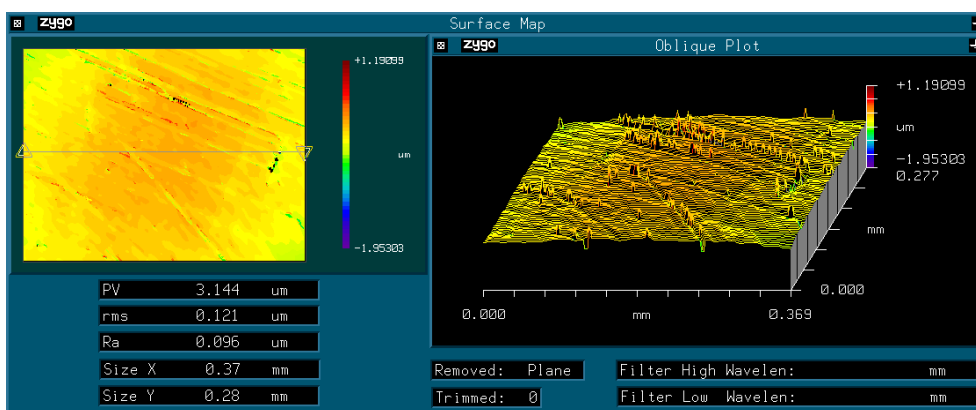


**Fig. 3.2.** Tin polycrystal surface after mechanical polishing.

### 3.2.2. Borate buffer solution

All the electrochemical experiments presented within this work were done in a boric/borate buffer solution at pH= 7.5. The solution was prepared by mixing  $\text{H}_3\text{BO}_3$  0.35 M and  $\text{Na}_2\text{B}_4\text{O}_7$  0.0375 M. Prior to the electrochemical experiments, the solution was bubbled with Argon gas in order to remove the oxygen, but no bubbling was necessary during the experiments.

## 3.3. Reagents

Here we give a list of all the reagents used throughout this work, either in the metal addition or in the electrochemistry section. It must be stated that all solutions have been prepared with, at least, p.a. grade reagents and triply distilled water, which is also used for all water rinses. Products used are:

**From Alfa:**  $\text{PdCl}_2$ (99.9%),  $\text{SnCl}_2$ (99%),  $(\text{NH}_4)_2\text{PtCl}_4$ (99.9%),  $\text{K}_2\text{RuCl}_5 \cdot \text{H}_2\text{O}$  (99.99%),  $\text{NiCl}_2 \cdot 6 \text{H}_2\text{O}$  (99.95%),  $\text{NaH}_2\text{PO}_2 \cdot \text{H}_2\text{O}$ ,  $\text{NH}_4\text{OH}$  (5 N Standardised solution) and  $\text{SnO}_2$ (99.9%)

**From Merck:**  $\text{Na}_2\text{B}_4\text{O}_7 \cdot 10 \text{H}_2\text{O}$  (p.a.),  $\text{H}_3\text{BO}_3$  (p.a.),  $\text{HCl}$ (37% fuming, p.a.),  $\text{H}_2\text{SO}_4$ (95-97%, Selectipur).

**From Aldrich:**  $\text{SnSO}_4$ (95%).



## **4. Metal Addition Methods** **On Tin Oxide**



## **4. METAL ADDITION METHODS ON TIN OXIDE**

In this section, we will present the results of the characterisation of the different samples prepared for their study as gas sensors, together with the discussion of the main catalyst addition features for the different cases studied.

As the main aim of this work has been to develop a new addition method of catalysts on tin oxide, we will begin describing the general characterisation of pure tin oxide nanoparticles used as base material within this work. Afterwards, we will present the results obtained for the characterisation of catalyst addition with classical addition processes, used for the sake of comparison with the new addition process, ending with the characterisation of the materials obtained with the developed addition method.

Afterwards, we will present the catalytic activity of conversion of CO to CO<sub>2</sub> of the different samples to show some practical applications of the developed materials, finishing the chapter with the discussion of the presented results.

### **4.1. Characterisation**

The results presented along this section concern the physicochemical characterisation of the samples by means of the different techniques previously described, i.e. XRD, Raman, XPS, TEM and ICP and, for all the samples, the results were analysed following the same procedure. Thus, the cell parameters were calculated from the XRD spectra using the CELREF program, while the grain size was calculated applying the Debye-Scherrer equation. With respect to the IR and Raman peaks, they were fitted using a Lorentzian function with the SC program. Raman shifts were corrected with respect to the silicon Raman band, that was fixed at 520 cm<sup>-1</sup>. XPS shifts and valence bands were corrected using the carbon 1s peak as reference and giving it a value of 284.5 eV [149]. Fittings were performed considering 80/20 % Gaussian/Lorentzian orbital peaks and Shirley baselines [173]. TEM image processing was made using DigitalMicrograph and Photoshop software.

#### **4.1.1. Pure SnO<sub>2</sub>**

For the sake of comparison, the commercial tin dioxide used as base material during this work has been characterised by XRD, Raman, XPS and TEM. Thus, figure 4.1 shows the XRD spectra of the base material at all the annealing temperatures used within this work. The pattern of this blank sample is that of cassiterite [174]. The (110) surface of SnO<sub>2</sub> is energetically the most stable, explaining why this orientation is the predominant crystal face found in polycrystalline samples. No substantial changes are observed in the XRD spectra, probably due to the fact that the used material has been stabilised with an annealing treatment previously to its commercialisation. This is supported by the small changes of the cell parameters calculated for all these samples, that are showed in Table 4.1. The mean grain size calculated from the Debye-Scherrer equation for the used SnO<sub>2</sub> is of 62 ± 2 nm for the non-annealed samples. This size increases slightly with the annealing temperature, reaching a mean grain size of 65 ± 1 nm in the samples annealed at 800 °C.

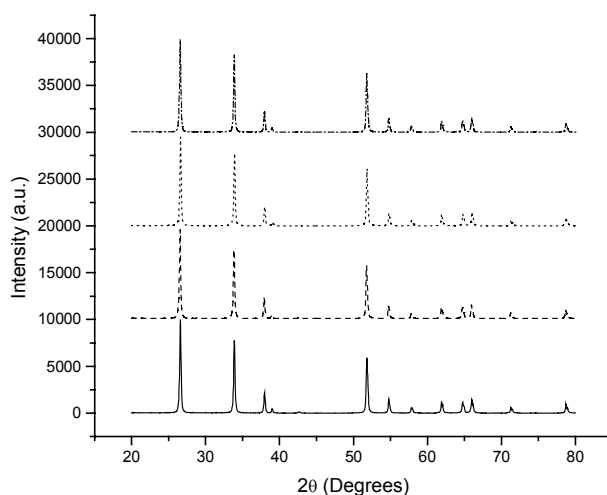


**Fig. 4.1.** XRD spectra of the used SnO<sub>2</sub>: — , non-annealed; --- , annealed at 200 °C; ..... , annealed at 450 °C; -.-.- , annealed at 800 °C.

	a (Å)	c (Å)	Grain size (211) (nm)
<b>Non-annealed</b>	4.735	3.185	62.5
<b>200 °C</b>	4.735	3.185	64.7
<b>450 °C</b>	4.736	3.185	65.1
<b>800 °C</b>	4.735	3.185	65.7

**Table 4.1.** Calculated cell parameters and grain size of pure SnO<sub>2</sub> after different annealing treatments.

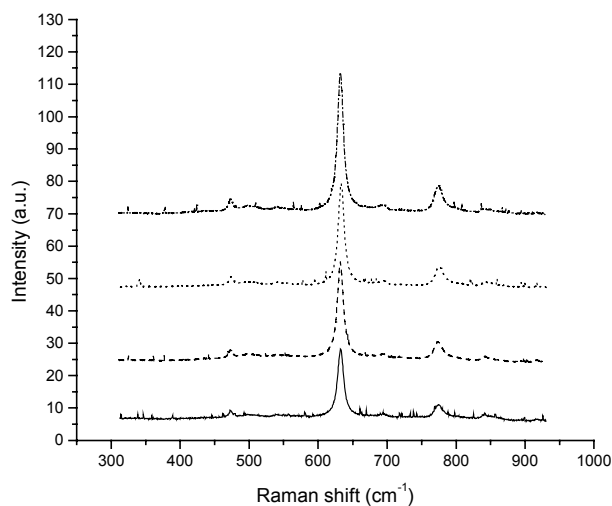


**Fig. 4.2.** Raman spectra of pure SnO<sub>2</sub> with different annealing treatments: — , non-annealed; --- , annealed at 200 °C; ..... , annealed at 450 °C; -.-.- , annealed at 800 °C.

With respect to Raman, only small changes were detected when changing the annealing temperature. Thus, the Raman spectra of these samples are shown in fig. 4.2. Raman spectra of the whole set of samples show, among all the possible SnO<sub>2</sub> Raman bands [29], those bands currently detected, i.e. A<sub>1g</sub> (630 cm<sup>-1</sup>), B<sub>2g</sub> (774 cm<sup>-1</sup>) and E<sub>1g</sub> (472 cm<sup>-1</sup>) [175] and only a small shift of the position of A<sub>1g</sub> peak to higher values and a small decrease of the width of this peak when increasing the annealing temperature were observed, probably due to a slight change of the material, as discussed in XRD.

The XPS shift of the Sn 3d peak was that of SnO<sub>2</sub> and no other component was detected and, with respect to the valence band spectra, all of them were also similar and two are showed in fig. 4.3. The observed spectra coincide with those reported elsewhere [176], where the oxygen 2p and 2s orbitals give the dominant contribution.

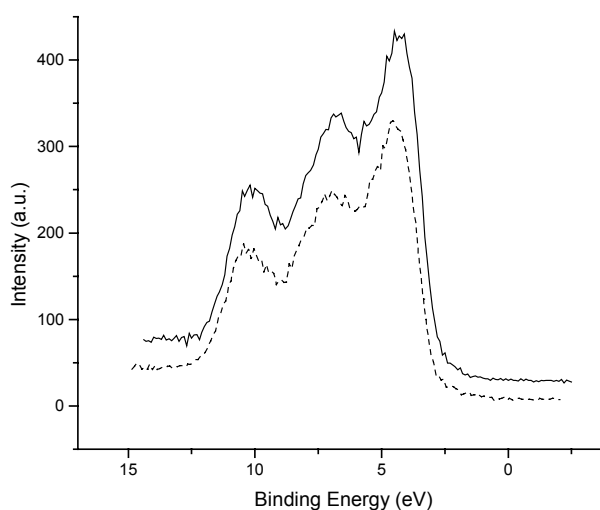


**Fig. 4.3.** XPS valence band spectra of pure SnO<sub>2</sub> annealed at different temperatures: —, 200 °C; ---, 800 °C

A typical TEM image of pure SnO<sub>2</sub> nanoparticles used within this work as base material is shown in fig. 4.4. It can be observed that the material is in form of nanoparticles with a crystalline structure of cassiterite.

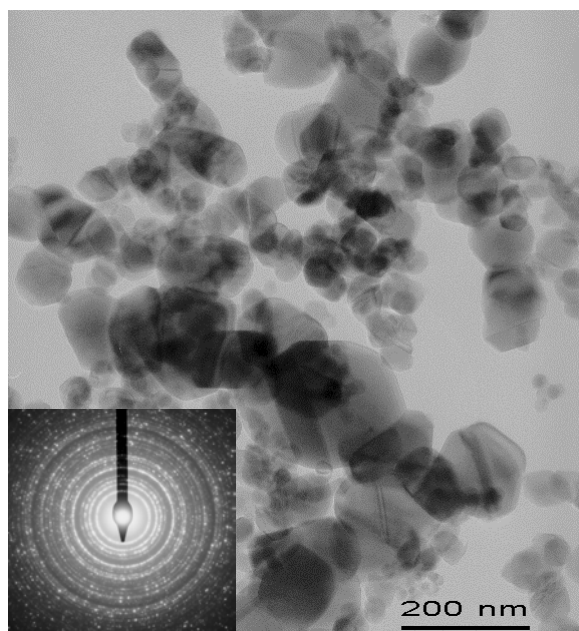


**Fig. 4.4.** TEM image of  $\text{SnO}_2$  nanoparticles. The inset shows the diffraction spectra of the nanoparticles, that confirms the cassiterite structure of the material.

### 4.1.2. Classical addition processes

In this section, the characterisation of the materials obtained with the classical addition methods is presented. As has been discussed in the Introduction section, the classical additives for this kind of materials are Pd and Pt, and impregnation is the most used addition method. There are a lot of variations of the impregnation method, but here we have only studied two impregnation processes, one with evaporation to dryness and another one with filtering of the powders after impregnation with a solution of the metal salt.

#### 4.1.2.1. Impregnation with Pd.

##### 4.1.2.1.1. Impregnation without evaporation to dryness

Nominal Pd/Sn (atomic%)	Annealing T (°C)	Pd found/nominal Pd (%)	Pd inserted/total Pd (%)
1	-	33.99	-
1	800	32.88	45.37
5	-	14.92	-
5	800	4.93	63.22

**Table 4.2.** ICP results of the samples impregnated without evaporation to dryness.

In this case, the most important results are those from ICP, summarised in table 4.2. It can be observed that the efficiency of this method is very low, thus obtaining a real percentage of catalyst much lower than the nominal one. Moreover, the samples annealed at 800 °C present an interesting feature: there is a great amount of Pd that only dissolves after the third chemical step of the dissolution process applied to perform the ICP analysis.

The meaning of this Pd, that is labelled as “Pd inserted” in table 4.2, and that is observed independent of the addition process, will be discussed below.

Thus, because of the low quantity of metal added, the XRD spectra show no additional phases corresponding to the metal added. The SnO<sub>2</sub> cell parameters of table 4.3. also show no significant variation.

Nominal Pd (at.%)	Annealing T (°C)	a (Å)	c (Å)
1	-	4.735	3.185
5	-	4.735	3.185
1	450	4.735	3.185
5	450	4.735	3.185
1	800	4.736	3.185
5	800	4.735	3.185

**Table 4.3.** Cell parameters of the samples calculated from the XRD spectra.

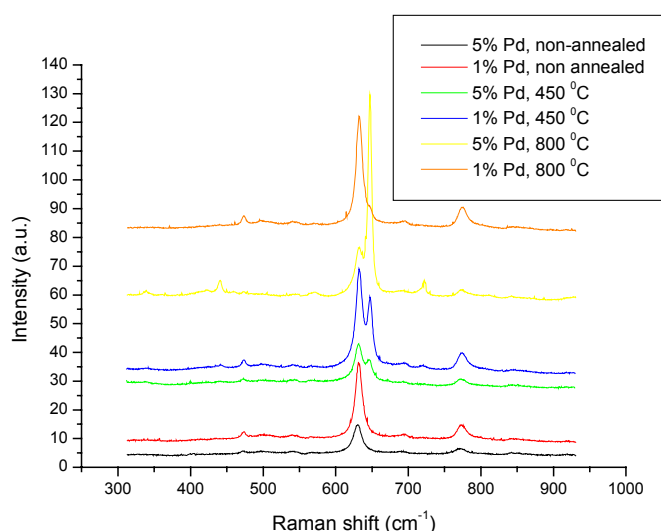


**Fig. 4.5.** Raman spectra of the samples impregnated with Pd. See the inset of the figure, where the nominal metal concentrations and the annealing temperature are detailed.

With respect to the Raman spectra, several features can be observed. First of all, in spite of the low concentrations of additive present in the samples, an additional Raman band that can be associated with the catalyst appears after annealing (see fig.4.5.). This Raman band at 650cm<sup>-1</sup> is attributed to the most intense and practically the unique visible PdO Raman band [177] and is narrower after annealing at higher temperature. It can be seen (fig. 4.6.) that both this band and the A<sub>1g</sub> band of SnO<sub>2</sub> shift to lower values at higher additive concentration, thus indicating a possible interaction between the additive and the base material. The most important values obtained from the fitting of the Raman spectra are summarised in table 4.4.

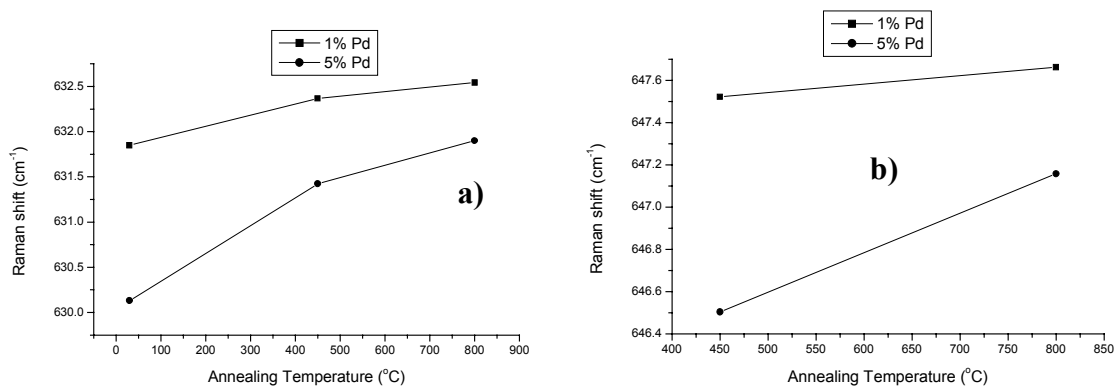


**Fig. 4.6.** Raman shifts of: (a) SnO<sub>2</sub> A<sub>1g</sub> band: —■—, nominal 1 atom % Pd; —●—, nominal 5 atom % Pd; (b) PdO band: —■—, nominal 1 atom % Pd; —●—, nominal 5 atom % Pd.

Additive conc. (atomic %)	Annealing T (°C)	A <sub>1g</sub> Raman shift (cm <sup>-1</sup> )	A <sub>1g</sub> width (cm <sup>-1</sup> )	PdO Raman shift (cm <sup>-1</sup> )	PdO width (cm <sup>-1</sup> )	PdO/A <sub>1g</sub> relative area
1	-	631.9	11.5	-	-	-
1	450	632.4	11.1	647.5	7.7	44.6
1	800	632.5	10.5	647.7	6.1	3.1
5	-	630.1	14.1	-	-	-
5	450	631.4	12.8	646.5	9.8	36.4
5	800	631.9	12.8	647.2	5.8	208.1

**Table 4.4.** FWHM and Raman shifts of the SnO<sub>2</sub> A<sub>1g</sub> and PdO Raman bands.

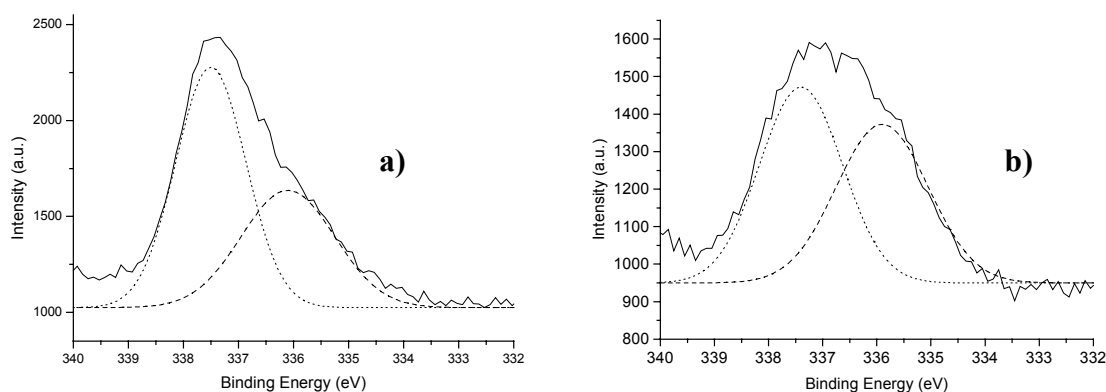


**Fig. 4.7.** XPS spectra and fitting results of the sample with 5% nominal Pd: (a) non-annealed: —, acquired spectrum; ---, Pd<sup>2+</sup>; ·····, PdCl<sub>2</sub>; (b) annealed at 800 °C: —, acquired spectrum; ---, PdO; ·····, PdO<sub>2</sub>.

In the XPS spectra, the Pd is also detected. In non-annealed samples, it is present only in +2 oxidation state (both as Pd<sup>+2</sup> and as PdCl<sub>2</sub> (3d<sub>5/2</sub> peak at 337.2 eV) [178]), and after annealing at sufficiently high temperature, it is present as a mixture of PdO (3d<sub>5/2</sub> peak at 336.1 eV) [179] and PdO<sub>2</sub> (3d<sub>5/2</sub> peak at 337.6 eV) [180] (see fig.4.7.). With respect to the valence band, surface states at the top of the valence band, below the Fermi level, are observed (see fig. 4.8) and, as previously reported [35], can be associated with the catalyst. The density of states increases, of course, with catalyst concentration. It must be stated that the shape and behaviour of the valence bands was similar to that showed in fig. 4.8 independently of the annealing temperature. Table 4.5 summarises some of the features observed in these samples. With respect to the presented results, it is worth to comment that, as all XPS results presented throughout this work, all the oxidation state values are taken in non-sputtered samples because the sputtering process modifies the sample, and no quantitative discussion of the percentage of the different oxidation states will be presented. Only the atomic concentration values are present after sputtering but these values (both before and after sputtering) are only orientative as they are affected by the fact that XPS only gives a superficial analysis. Nevertheless, some interesting features can be inferred from these values. Thus, for example, it can be observed that chlorides are only completely eliminated after annealing at 800 °C. Moreover, the Pd/Sn ratio is always lower after sputtering, thus indicating that the Pd added is mainly on the surface or the first superficial layers of the SnO<sub>2</sub> nanoparticles.

With respect to the oxidation states, at 450 °C it is very difficult (with the results obtained in this work) to discern whether the peak observed around 337.5 eV is due to PdCl<sub>2</sub>, PdO<sub>2</sub> or to a mixture of both compounds. Thus, to simplify, throughout this work it has been assigned only to PdO<sub>2</sub>. The evidence supporting this assignment is the fact that the Raman spectra of the samples annealed at 450 °C show a PdO band even in this samples, where a little amount of Pd is present. Moreover, in samples obtained with evaporation to dryness, no bands associated to chlorides are detected at 450 °C, while they are clearly detected in non-annealed samples, thus indicating that a much lower amount (if there is any) of PdCl<sub>2</sub> is present at this annealing temperature.

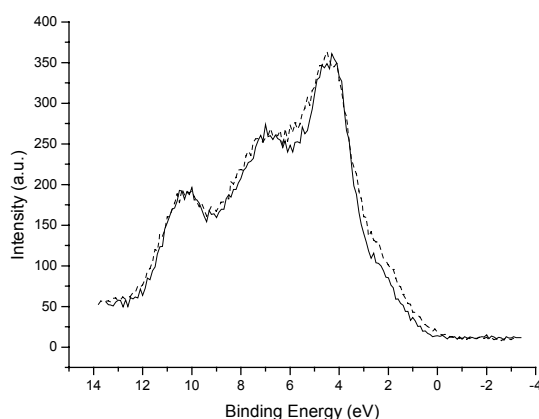


**Fig. 4.8.** Valence band spectra of the samples annealed at 800 °C: — , nominal 1 atom % Pd; --- , nominal 5 atom % Pd.

Nominal Pd (at.%)	Annealing T (°C)	Cl (at.%)	Pd (at.%)	Sn (at.%)	Pd/Sn (at.%)
1	-	1.3/ 0.6*	0.8/ 0.5*	28.7/ 41.2*	2.8/ 1.3*
1	450	1.4/ 0.5*	0.8/ 0.5*	29.3/ 40.7*	2.6/ 1.1*
1	800	0/ 0*	1/ 0.5*	30.7/ 40.6*	3.2/ 1.3*
5	-	3.2/ 1.5*	2.4/ 1.4*	29.1/ 40.3*	8.2/ 3.4*
5	450	1.8/ 1.1*	2.1/ 1.2*	26.5/ 40.6*	8/ 3*
5	800	0/ 0*	1.2/ 0.8*	29.5/ 40.3*	4.2/ 2*

\*Values after sputtering.

**Table 4.5.** Atomic concentration results obtained from the XPS data of the samples.

#### 4.1.2.1.2. Impregnation with evaporation to dryness

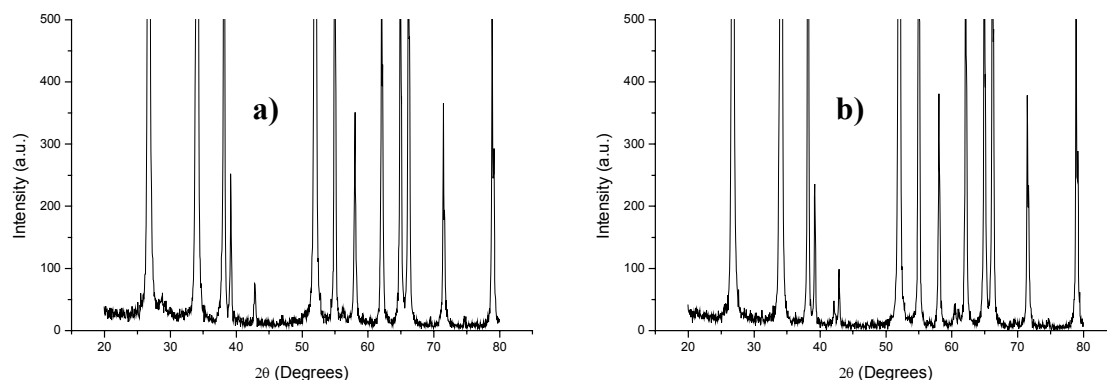


**Fig. 4.9.** XRD spectra of the sample with nominal 5% Pd: (a) non-annealed; (b) annealed at 800 °C.

The XRD results of the samples with highest additive concentration are shown in fig. 4.9. In the non-annealed samples, apart from the XRD peaks corresponding to polycrystalline SnO<sub>2</sub> [174] there are no additional peaks observed. After annealing at 800 °C, the peaks corresponding to PdO [181] are present, as can be observed in figure 4.9.b. The evidence of PdO after annealing at sufficiently high temperature is in agreement with the results reported for samples obtained by using other addition techniques [177,182,183]. The cell parameters of SnO<sub>2</sub> have been calculated for these samples and are presented in Table 4.6. No clear variation of the cell parameters is observed, neither with the additive concentration nor with the annealing temperature.

Nominal Pd (at.%)	Annealing T ( °C)	a (Å)	c (Å)
1	-	4.738	3.187
5	-	4.736	3.186
1	450	4.736	3.185
5	450	4.735	3.185
1	800	4.736	3.186
5	800	4.738	3.186

**Table 4.6.** Cell parameters calculated from the fitting of the XRD spectra.

With respect to the Raman spectra, they are shown in figure 4.10. The non-annealed samples present the Raman bands corresponding to SnO<sub>2</sub> and bands corresponding to PdCl<sub>2</sub> (bands at 300 cm<sup>-1</sup>, [142]), while the annealed samples present the Raman bands of SnO<sub>2</sub> and of PdO. This band is present both after annealing at 450 and 800 °C, although its relative area is greater at higher annealing temperatures. The SnO<sub>2</sub> and PdO bands have a shift similar to that presented in the case of samples not evaporated to dryness.

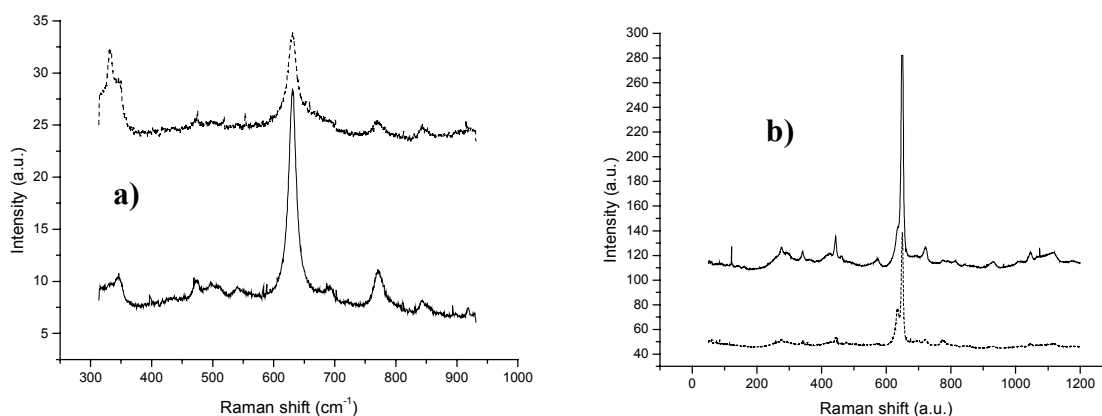


**Fig. 4.10.** Raman spectra of the samples: (a) non-annealed: — , nominal 1 atom % Pd; ---- , nominal 5 atom % Pd; (b) annealed at 800 °C: — , nominal 1 atom % Pd; --- , nominal 5 atom % Pd.

The XPS and TEM characterisation of these samples have not been performed due to the extensive bibliography that discusses the results obtained for this kind of samples. Thus, in general, the palladium added by impregnation in these samples is present mainly as PdCl<sub>2</sub> without annealing, while after annealing in air there is the presence of PdO and PdO<sub>2</sub>, while the valence band spectra obtained for these samples is similar to that obtained in the previous subsection. An extensive discussion of the results obtained in this kind of samples has been also presented and performed in our investigation group [57,124]. It must be stated that, at least in our case, hardly any nanocluster of the added catalyst is found on the tin oxide surface if no reduction processes are applied.

The ICP results showed in table 4.7. state that the efficiency of palladium addition to SnO<sub>2</sub> is very high at all annealing temperatures, although it is a little less after annealing. Moreover, the ICP results show the presence of a great amount of “Pd inserted”, as also observed with the addition method presented above.

Nominal Pd/Sn (atomic%)	Annealing T (°C)	Pd found/nominal Pd (%)	Pd inserted/total Pd (%)
1	-	92	-
1	800	78.1	72.7
5	-	86.2	-
5	800	58.1	90.1

**Table 4.7.** Summary of the ICP results obtained for these samples.

#### 4.1.2.2. Impregnation with Pt.

##### 4.1.2.2.1. Impregnation without evaporation to dryness.

In this case, the most important results are those from ICP. No platinum is detected, indicating that the efficiency of this method is even lower than in the case of palladium, thus obtaining a real percentage of metal much lower than the nominal one (in fact, this means that we have added no catalyst). This implies that no changes are observed in these samples with respect to the undoped ones presented above. Thus, the XRD spectra show no additional phases corresponding to the metal added. The SnO<sub>2</sub> cell parameters of table 4.8. also show no significant variation.

Nominal Pt (at.%)	Annealing T (°C)	a (Å)	c (Å)
2	-	4.736	3.185
10	-	4.736	3.185
2	450	4.735	3.185
10	450	4.735	3.185
2	800	4.735	3.185
10	800	4.735	3.185

**Table 4.8.** Cell parameters calculated after different annealing treatments.

With respect to the Raman spectra, it can only be observed that the A<sub>1g</sub> band of SnO<sub>2</sub> slightly shifts to higher values and is slightly narrower at higher annealing temperature, and these behaviours are independent from the additive concentration (see fig. 4.11.) and are coincident with the features detected for pure SnO<sub>2</sub>. The most important values obtained from the Raman spectra are summarised in table 4.9.

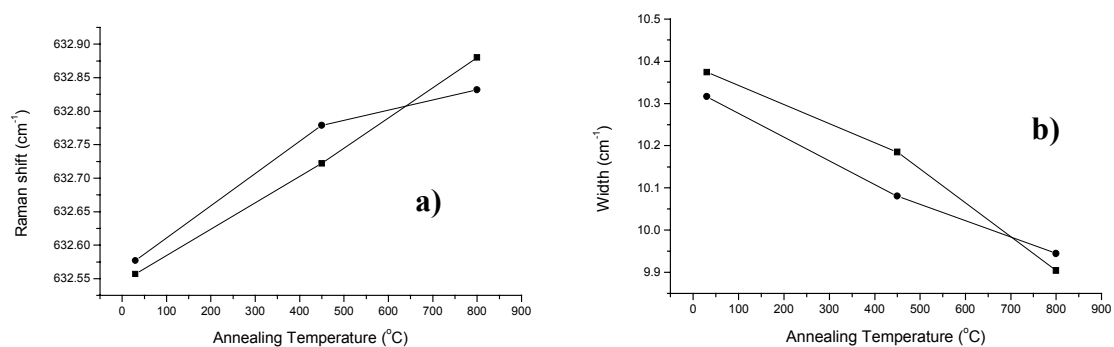


**Fig. 4.11.** Results of the fitting of the  $\text{SnO}_2$   $A_{1g}$  Raman band: (a) Shift:  $\blacksquare$ , nominal 2 at. % Pt;  $\bullet$ , nominal 10 at. % Pt; (b) Width:  $\blacksquare$ , nominal 2 at. % Pt;  $\bullet$ , nominal 10 at. % Pt.

Additive conc. (atomic %)	Annealing T (°C)	$A_{1g}$ Raman shift (cm <sup>-1</sup> )	$A_{1g}$ width (cm <sup>-1</sup> )
2	-	632.6	10.4
2	450	632.7	10.2
2	800	632.9	9.9
10	-	632.6	10.3
10	450	632.8	10.1
10	800	632.8	9.9

**Table 4.9.** Fitting values of the Raman spectra.

In the XPS spectra, the platinum is not detected, thus confirming that the efficiency of this addition method is inexistent.

#### 4.1.2.2.2. Impregnation with evaporation to dryness

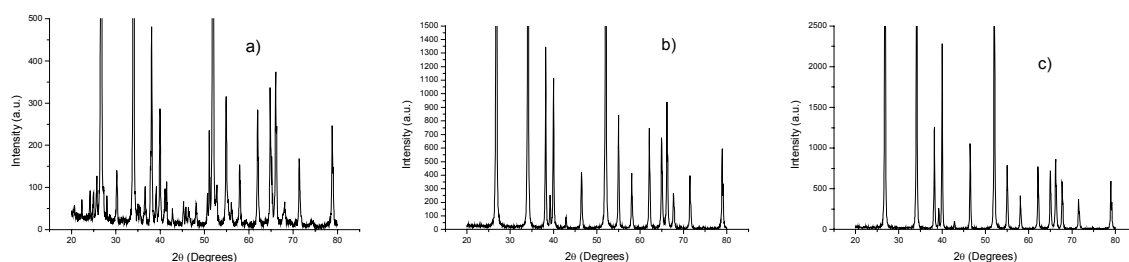


**Fig. 4.12.** XRD spectra of the sample with nominal 10% Pt: (a) non-annealed; (b) annealed at 450 °C and (c) annealed at 800 °C.

The XRD results of the samples with highest additive concentration are shown in fig. 4.12. In the non-annealed samples, apart from the XRD peaks corresponding to polycrystalline  $\text{SnO}_2$ , additional peaks corresponding to chlorides, mainly a mixture of  $\text{PtCl}_2$  and  $(\text{NH}_4)_2\text{PtCl}_4$  [184,185], can be observed. After annealing at 450 °C, only the

peaks corresponding to metallic platinum [186] are observed and, increasing the annealing temperature, the peaks narrow, thus indicating an increase of the platinum cluster size. The cell parameters of SnO<sub>2</sub> have been calculated for these samples and are presented in Table 4.11. No clear variation of the cell parameters is observed, neither with the additive concentration nor with the annealing temperature.

Nominal Pt (at.%)	Annealing T (°C)	a (Å)	c (Å)
2	-	4.738	3.187
10	-	4.737	3.186
2	450	4.736	3.186
10	450	4.736	3.186
2	800	4.738	3.187
10	800	4.737	3.186

**Table 4.11.** Cell parameters resulting from the fitting of the XRD spectra.

With respect to the Raman spectra, they are shown in figure 4.13. The non-annealed samples present the Raman bands corresponding to SnO<sub>2</sub> and bands corresponding to chlorides at 100 and 300 cm<sup>-1</sup> (PtCl<sub>2</sub>) [142], while the annealed samples only present the Raman bands of SnO<sub>2</sub>. Similar influence of the additive concentration on the SnO<sub>2</sub> A<sub>1g</sub> peak as in the case of samples not evaporated to dryness discussed above is also found in these spectra.

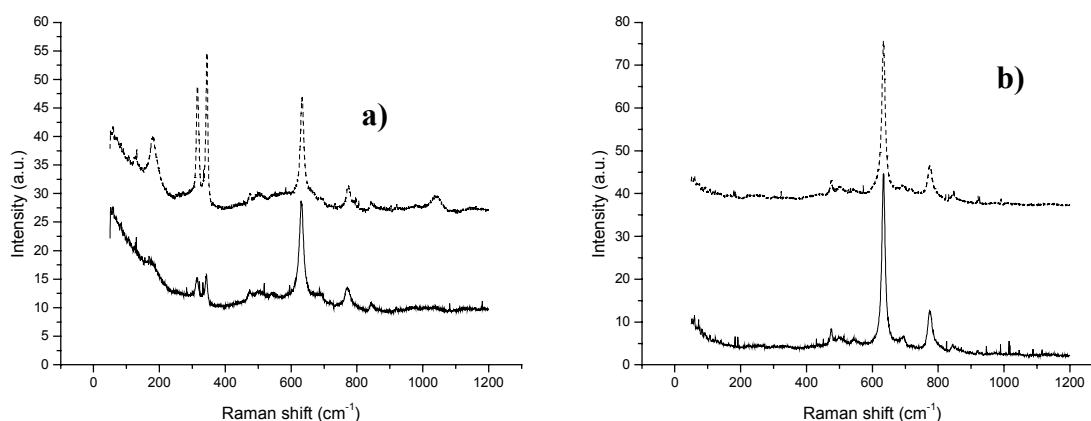


**Fig. 4.13.** Raman spectra of the samples: (a) non-annealed: — , nominal 2 atom % Pt; --- , nominal 10 atom % Pt; (b) nominal 10 atom % Pt: — , annealed at 450 °C; --- , annealed at 800 °C.

The XPS and TEM characterisation of these samples have not been done due to the extensive bibliography that discusses the results obtained for this kind of samples. Thus, in general, the platinum added by impregnation is present mainly as PtCl<sub>2</sub> without annealing, while after annealing in air there is the presence of metallic Pt, PtO and PtO<sub>2</sub>, with relative percentages depending on the annealing temperature, while the valence band spectra obtained for these samples is similar to that obtained with palladium. An extensive discussion of the results obtained in this kind of samples has been also presented and performed in our investigation group [57,124]. It must be stated that, at least in our case, hardly any nanocluster of the added catalyst is found on the tin oxide surface.

The ICP results showed in table 4.12. state that the efficiency of platinum addition to SnO<sub>2</sub> is very high at all annealing temperatures, although it is a little less after annealing. Moreover, the ICP results show the presence in the annealed samples of only a small amount of platinum that is dissolved in the third chemical step of the dissolution process, in contrast with the results obtained in the case of palladium.

Nominal Pt/Sn (atomic%)	Annealing T (°C)	Pt found/nominal Pt (%)	Pt in third process/total Pt (%)
2	-	69.2	-
2	800	56.3	4.8
10	-	94.8	-
10	800	62.7	1.2

**Table 4.12.** Summary of the concentration of the elements present in these samples obtained from ICP results.

### 4.1.3. Electroless addition

#### 4.1.3.1. Addition of Pd using Sn(II) as reductor

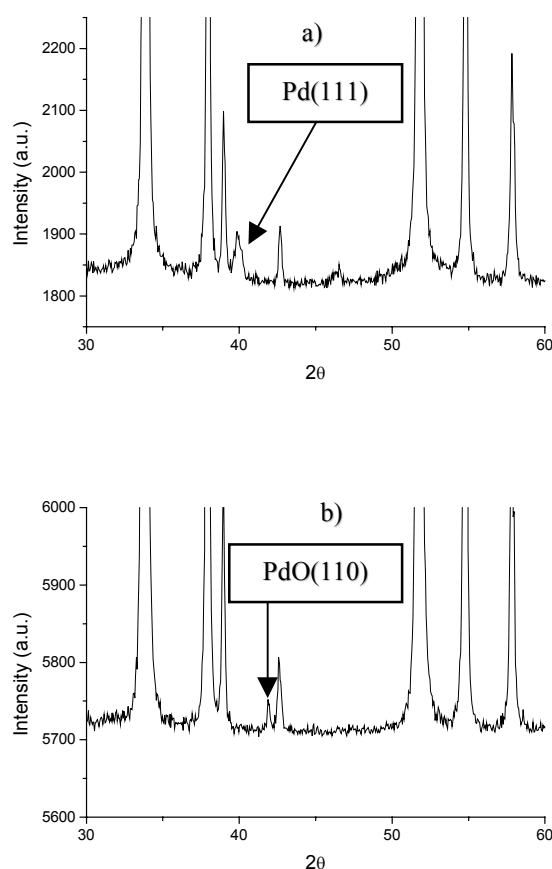


**Figure 4.14.** XRD diffractograms of two samples obtained from solutions with nominal 5% atomic Pd and a SnCl<sub>2</sub> concentration 10 times the stoichiometric ratio: a) non-annealed; b) annealed at 800 °C.

XRD patterns of two samples with the highest catalyst percentage (Figure 4.14) show the diffractogram obtained for the blank sample (the pattern of this blank sample is that of cassiterite [174]) with some additional phases corresponding to the added catalyst. With respect to the added catalyst, in the non-annealed sample only the peaks corresponding to metallic palladium [187] are detected (figure 4.14a) and in the one annealed at 800 °C only those of PdO [182] are present (figure 4.14b). The evidence of PdO after annealing at sufficiently high temperature is in agreement with the results reported for samples obtained by using other addition techniques [177,182,183]. In the samples with lower nominal catalyst concentrations no XRD palladium phases have been detected because the abundance of these phases lies below the XRD detection limit but the same behaviour is expected, as we will show below. With respect to the adjustment of the lattice parameters from the XRD spectra of these samples, they are summarised in table 4.13. No significant changes are observed neither with the catalyst concentration nor with the annealing temperature.

Nominal Pd (at.%)	Reductor ratio (atomic)	Annealing T ( °C)	a (Å)	c (Å)
0.1	1	-	4.736	3.185
0.1	10	-	4.736	3.185
1	1	-	4.736	3.186
1	10	-	4.735	3.185
5	1	-	4.735	3.185
5	10	-	4.736	3.186
0.1	1	200	4.735	3.185
0.1	10	200	4.736	3.185
1	1	200	4.735	3.185
1	10	200	4.736	3.185
5	1	200	4.735	3.185
5	10	200	4.735	3.184
0.1	1	450	4.736	3.185
0.1	10	450	4.736	3.186
1	1	450	4.735	3.185
1	10	450	4.735	3.185
5	1	450	4.735	3.185
5	10	450	4.737	3.186
0.1	1	800	4.736	3.185
0.1	10	800	4.735	3.185
1	1	800	4.735	3.185
1	10	800	4.736	3.185
5	1	800	4.736	3.185
5	10	800	4.735	3.185

**Table 4.13.** Cell parameters obtained after fitting the different XRD spectra.

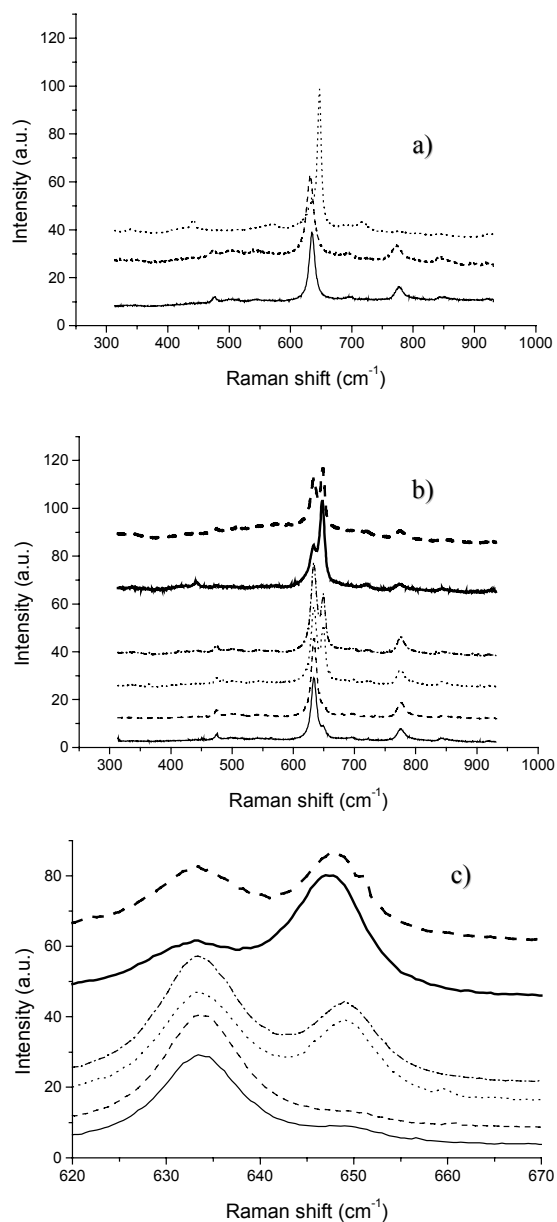
Raman spectra of the whole set of samples show, among all the possible SnO<sub>2</sub> Raman bands [29], those bands currently detected, i.e. A<sub>1g</sub> (630 cm<sup>-1</sup>), B<sub>2g</sub> (774 cm<sup>-1</sup>) and E<sub>1g</sub> (472 cm<sup>-1</sup>) [175] (fig. 4.15). In the added catalyst samples, no additional Raman band is detected in the non-annealed samples. This means that the main part of the palladium in these samples is present as metallic state because of the high reflectivity of metals to the laser radiation used in Raman measurements. The presence of other palladium compounds (like PdCl<sub>2</sub>) at sufficiently high concentration would have shown additional Raman bands. An additional Raman band at 650cm<sup>-1</sup> is obtained when the sample is annealed either at

450 or 800 °C, which is attributed to the most intense and practically the unique visible PdO Raman band [177]. The area ratio of this band with respect to that of SnO<sub>2</sub> A<sub>1g</sub> Raman band increases with catalyst concentration (figure 4.15b). The two other SnO<sub>2</sub> Raman bands decrease their area as the catalyst concentration increases until they disappear and, as a result, the SnO<sub>2</sub> Raman spectra is completely masked (figure 4.15a). In addition, the PdO and the SnO<sub>2</sub> A<sub>1g</sub> Raman bands shift to more negative values as the catalyst concentration increases (figure 4.15c). The shift in figure 4.15c allows us to speculate about the possible incorporation of palladium to the SnO<sub>2</sub> structure. The complete Raman results (for all catalyst concentrations and annealing temperatures) are summarised in table 4.14 where it can be observed that, at high catalyst concentration and high annealing temperature, the width of the SnO<sub>2</sub> A<sub>1g</sub> band is incremented, probably because of the insertion of Pd.

Additive conc. (atomic %)	Reductor Ratio	Annealing T (°C)	A <sub>1g</sub> Raman shift (cm <sup>-1</sup> )	A <sub>1g</sub> width (cm <sup>-1</sup> )	PdO Raman shift (cm <sup>-1</sup> )	PdO width (cm <sup>-1</sup> )	PdO/A <sub>1g</sub> relative area
0.1	1	-	631.6	11.1	-	-	-
0.1	10	-	631.5	11.3	-	-	-
0.1	1	200	632.1	10.7	-	-	-
0.1	10	200	632.1	10.7	-	-	-
0.1	1	450	632.4	10.5	648.4	7.6	0.1
0.1	10	450	632.4	10.4	648.6	7.1	0.1
0.1	1	800	632.4	10.4	-	-	-
0.1	10	800	632.2	10.7	-	-	-
1	1	-	631.6	11.0	-	-	-
1	10	-	630.8	11.2	-	-	-
1	1	200	631.8	11.2	-	-	-
1	10	200	630.9	11.7	-	-	-
1	1	450	632.1	11.3	647.7	7.5	0.5
1	10	450	632.1	10.9	647.8	7.8	0.4
1	1	800	631.8	11.4	646.7	6.8	0.2
1	10	800	632.0	11.1	646.5	5.7	0.1
5	1	-	630.0	10.4	-	-	-
5	10	-	629.4	11.9	-	-	-
5	1	200	630.0	12.2	-	-	-
5	10	200	629.3	12.5	-	-	-
5	1	450	631.2	13.6	646.0	8.6	1.3
5	10	450	631.6	13.3	646.5	7.4	0.7
5	1	800	630.7	21.2	645.1	8.4	2.7
5	10	800	631.0	21.3	645.0	6.8	2.6

**Table 4.14.** Summary of the parameters obtained after fitting the Raman spectra of the samples.

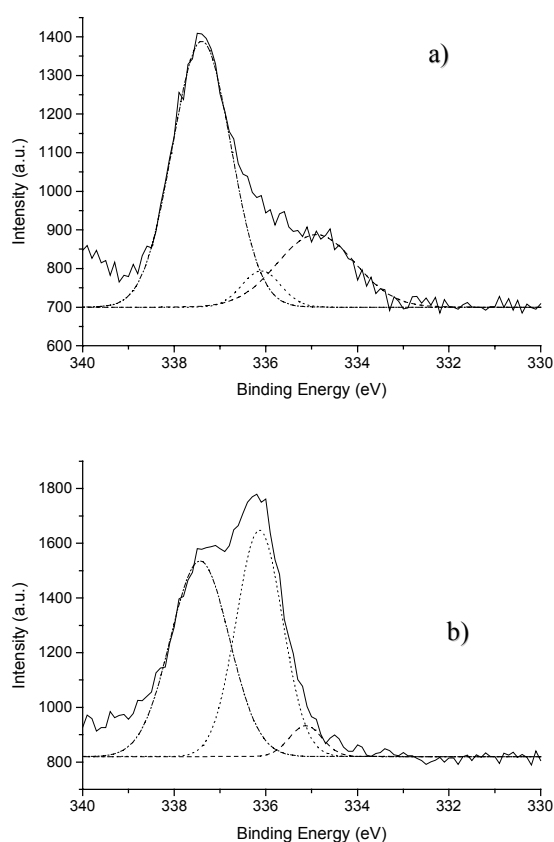
In order to know where the catalyst is distributed in the SnO<sub>2</sub> nanopowders, we have also investigated the XPS response of the set of prepared samples. The spectra of the sample with the highest catalyst concentration non-annealed and after annealing at 800 °C are shown in figure 4.16a and 4.16b respectively. The fitting results verify the presence of both metallic palladium (3d<sub>5/2</sub> peak at 335.1 eV) [188] and Pd(II) at any annealing temperature. Pd(II) is mainly present as chloride (3d<sub>5/2</sub> peak at 337.2 eV) [164] at low annealing temperatures and as PdO (3d<sub>5/2</sub> peak at 336.1 eV) [165] after annealing at 450 or 800 °C. After annealing at 800 °C, no chlorides are detected, and there is the additional presence of a higher oxidation state of Pd, i.e. PdO<sub>2</sub> (3d<sub>5/2</sub> peak at 337.6 eV) [166] that has not been detected in the bulk. It is difficult to discern whether PdO<sub>2</sub> is present at 450 °C, as the XPS peaks of PdCl<sub>2</sub> and PdO<sub>2</sub> have similar shifts.



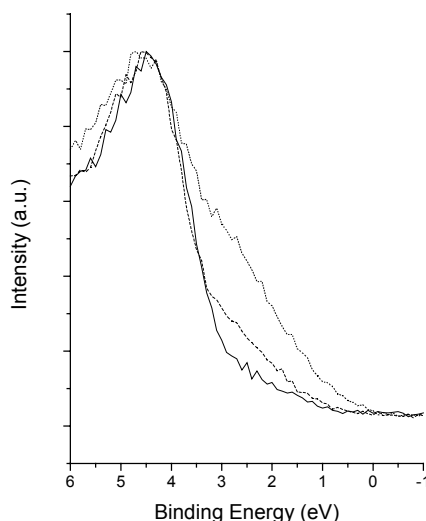
**Figure 4.15.** Raman spectra: a) Samples obtained from solutions with nominal 5% Pd a  $\text{SnCl}_2$  concentration 10 times the stoichiometric ratio: — non annealed; --- annealed at  $200^\circ\text{C}$ ; ..... annealed at  $800^\circ\text{C}$ ; b) Samples annealed at  $450^\circ\text{C}$ : — nominal 0.1% Pd, stoichiometric  $\text{SnCl}_2$ ; ----- nominal 0.1% Pd, a  $\text{SnCl}_2$  concentration 10 times the stoichiometric ratio; ..... nominal 1% Pd, stoichiometric  $\text{SnCl}_2$ ; ----- nominal 1% Pd, a  $\text{SnCl}_2$  concentration 10 times the stoichiometric ratio; ——— nominal 5% Pd, stoichiometric  $\text{SnCl}_2$ ; - - - nominal 5% Pd, a  $\text{SnCl}_2$  concentration 10 times the stoichiometric ratio; c) Is a zoom on b)

Table 4.15 summarises the atomic concentration values of the more significant elements. The fact that the obtained Pd/Sn ratio is always higher than the nominal one can be mainly due to the fact that, as XPS is a superficial analysis technique, this could mean that there is a greater amount of metal in the surface than in the bulk, and this is expected, as the nominal concentration has been calculated for the bulk of the sample, while the catalyst is added on its surface. It can also be observed that chlorides are completely eliminated only after annealing at 800 °C.

The valence band of the samples after annealing at 800 °C obtained by XPS are shown in figure 4.17. Surface states at the top of the valence band, below the Fermi level, are observed and, as previously reported [35], can be associated with the catalyst. The density of states increases, of course, with catalyst concentration. It must be stated that the shape and behaviour of the valence bands was similar to that showed in fig. 4.17 independently of the annealing temperature.



**Figure 4.16.** XPS spectra of the samples obtained from solutions with nominal 5% Pd a  $\text{SnCl}_2$  concentration 10 times the stoichiometric ratio: a) non annealed: — Acquired spectrum, --- Metallic palladium, ..... PdO, -.- PdCl<sub>2</sub>; b) annealed at 800 °C: — Acquired spectrum, ..... Metallic palladium, --- PdO, -.- PdO<sub>2</sub>.



**Figure 4.17.** VB spectra for samples with a  $\text{SnCl}_2$  concentration 10 times the stoichiometric ratio annealed at  $800\text{ }^\circ\text{C}$ : — nominal 0.1% Pd, ---- nominal 1% Pd and ..... nominal 5% Pd.

Figure 4.18 shows the TEM analysis of the sample with the highest catalyst concentration annealed at  $800\text{ }^\circ\text{C}$ . A mixture of metallic Pd and PdO on the surface of the  $\text{SnO}_2$  nanopowders is observed and palladium was demonstrated to be placed on the  $\text{SnO}_2$  surface forming metallic Pd and PdO nanoclusters. Figure 4.18.a) enlightens a PdO nanocluster placed on the surface of a  $\text{SnO}_2$  nanoparticle. Lattice spacing of nanocluster was calculated on the Fast Fourier Transform of TEM micrograph. In this case, we obtained  $2.15\text{ \AA}$ , corresponding to the (110) PdO planes. In figure 4.18.b) a Pd nanocluster was imaged also on the  $\text{SnO}_2$  nanoparticle surface. We applied several frequency filters on the FFT image in order to separate those planes corresponding to Pd from those corresponding to  $\text{SnO}_2$  planes. Lattice spacing were also calculated on FFT space and we obtained:  $3.35\text{ \AA}$  in the case of  $\text{SnO}_2$  corresponding to (110) planes and  $2.25\text{ \AA}$  in the case of Pd corresponding to (111) planes.

The density of Pd nanoclusters on  $\text{SnO}_2$  grain surface has been measured from the TEM images, obtaining  $(2.2 \pm 0.2) \cdot 10^{12}\text{ cm}^{-2}$ . Measurements performed in different  $\text{SnO}_2$  particles have shown a homogeneous distribution of these nanoclusters. After analysing over 100 nanoclusters we have found that approximately 90 % of them are oxidised (PdO), while just 10 % remain metallic (Pd). The mean diameter size obtained for these nanoclusters is  $24 \pm 2\text{ \AA}$  (see figure 4.18.c.). Following these results, we can conclude that the electroless method allowed us to obtain better nanocluster dispersion in the case of Pd that those impregnation methods reported before elsewhere [57,189]. As showed there, in the case of Pd loaded on  $\text{SnO}_2$  nanopowders using impregnation methods we hardly found nanocluster formation on semiconductor's surface.

Nominal Pd (at.%)	Reductor Ratio	Annealing T (°C)	Cl (at.%)	Pd (at.%)	Sn (at.%)	Pd/Sn (at.%)
0.1	1	-	0.9/ 0*	0.3/ 0.2*	29.5/ 39.7*	0.9/ 0.6*
0.1	10	-	0.9/ 0*	0.3/ 0.2*	29.5/ 40.2*	1/ 0.5*
0.1	1	200	0.5/ 0*	0.2/ 0.2*	27.9/ 34.6*	0.9/ 0.6*
0.1	10	200	0.6/ 0*	0.3/ 0.1*	24.4/ 30*	1.2/ 0.4*
0.1	1	450	0.7/ 0*	0.4/ 0.2*	31.6/ 39.5*	1.4/ 0.6*
0.1	10	450	1.6/ 0.7*	0.1/ 0*	31.1/ 40.2*	0.4/ 0*
0.1	1	800	0/ 0*	0.4/ 0.3*	29.3/ 35.1*	1.2/ 0.7*
0.1	10	800	0/ 0*	0.5/ 0.4*	30.9/ 34.6*	1.7/ 1*
1	1	-	1.3/ 0*	0.8/ 0.5*	28.9/ 40*	2.7/ 1.2*
1	10	-	2.7/ 1.5*	0.5/ 0.4*	28.1/ 40.2*	1.9/ 1*
1	1	200	1.5/ 0.6*	0.8/ 0.4*	31/ 40.3*	2.6/ 1*
1	10	200	2.6/ 1.1*	0.8/ 0.5*	29.5/ 39.6*	2.6/ 1.1*
1	1	450	1.6/ 1*	0.8/ 0.6*	22.8/ 39.5*	3.5/ 1.5*
1	10	450	1.1/ 0*	0.4/ 0.3*	30.3/ 39*	1.3/ 0.7*
1	1	800	0/ 0*	0.8/ 0.7*	30.8/ 33*	2.7/ 2.1*
1	10	800	0/ 0*	1/ 0.8*	30.5/ 32.8*	3.2/ 2.4*
5	1	-	2.6/ 1.3*	1.9/ 1.2*	26.5/ 40.6*	7.1/ 2.9*
5	10	-	5.4/ 3.9*	1.5/ 1.9*	25.2/ 38*	5.8/ 4.9*
5	1	200	2.8/ 1.9*	1.9/ 1.4*	27.4/ 38*	7.1/ 3.7*
5	10	200	6.1/ 3.5*	2.4/ 2*	28.8/ 36.5*	8.5/ 5.6*
5	1	450	3.1/ 1.5*	2/ 1.7*	27.8/ 38.4*	7.3/ 4.5*
5	10	450	4/ 1.7*	3.6/ 3*	27.2/ 38.1*	13.1/ 7.8*
5	1	800	0/ 0*	1.6/ 1.6*	28.2/ 32.3*	5.5/ 5*
5	10	800	0/ 0*	1.9/ 1.7*	28/ 32.7*	6.9/ 5.3*

\*Values after sputtering.

**Table 4.15.** Summary of the atomic concentration results obtained after integrating the areas of the XPS peaks for the different samples.

Nominal Pd/Sn (atomic%)	Nominal SnCl <sub>2</sub> /PdCl <sub>2</sub>	Annealing T (°C)	Pd found/nominal Pd (%)	SnCl <sub>2</sub> (atomic%)	Pd inserted/total Pd (%)
0.1	1	-	58.8	5e-4	0
0.1	10	-	91.5	0.002	0
1	1	-	23.6	0.002	0
1	10	-	63	0.005	0
5	1	-	45	0.013	0
5	1	800	34.4	7e-4	72
5	10	-	87	0.069	0
5	10	800	48	0.003	80

**Table 4.16.** Summary of the ICP results of the most relevant samples.

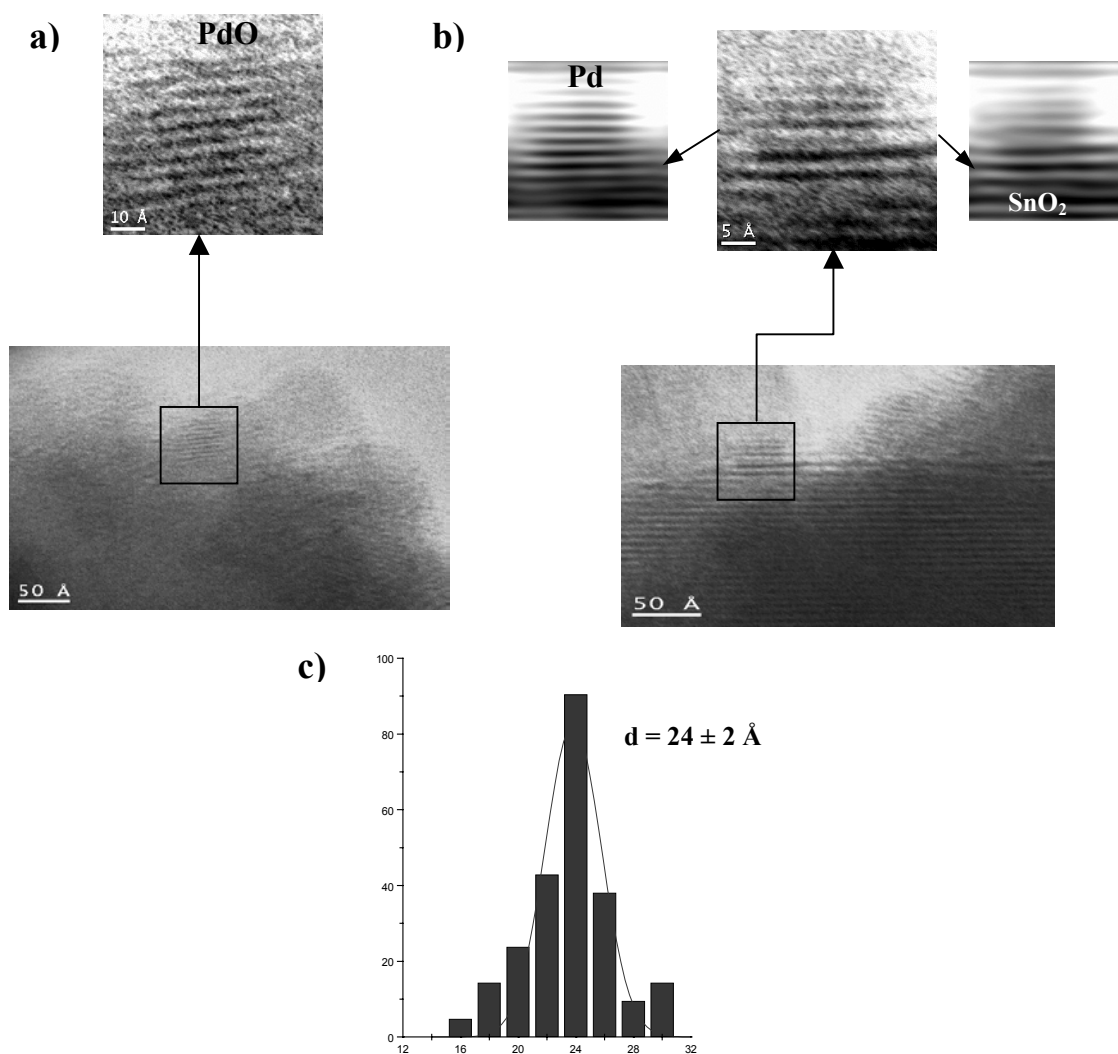


**Figure 4.18.** HRTEM images showing Pd and PdO phases in the sample with nominal 5% Pd and a SnCl<sub>2</sub> concentration 10 times the stoichiometric ratio annealed at 800 °C. **a)** PdO nanocluster embedded on a SnO<sub>2</sub> nanoparticle's surface. **b)** A Pd nanocluster on SnO<sub>2</sub> surface. The filtered images separating Pd and SnO<sub>2</sub> planes are also shown. **c)** Mean diameter size histogram of PdO nanoclusters measured on several HRTEM images.

With respect to the ICP results, they are summarised in Table 4.16. Only a few ICP partial results are reported for impregnated samples [190]. In our case, the results show that the efficiency of the electroless method for the catalyst addition to the SnO<sub>2</sub> nanopowders is very high, specially when using a higher reductor concentration, where we can find almost 90% of the expected Pd, although in these samples the percentage of species coming from the reductor salt present on the SnO<sub>2</sub> surface is also higher if no annealing was applied. Nevertheless, it should be stated that the chemical process described here is not able to distinguish between different oxidation states or compounds of palladium and, thus, we are referring to total palladium, (i.e., the total palladium quantity coming from either metallic Pd, PdCl<sub>2</sub>, PdO or any other palladium compound). This efficiency has the same average value than that obtained in classical impregnation and much higher than that of impregnation without evaporation to dryness. The efficiency decreases for annealed samples mainly due to the lost of catalyst during the heating process and also to the conversion of the reductor species, tin cations, to tin oxide because almost no reductor species are detected after annealing. Moreover, the ICP results showed that, in annealed samples at 800°C, most of the palladium is dissolved in the third chemical step described in the experimental section. It could be possible that palladium would be not soluble in aqua regia for a determined palladium compound but, although for example Pd-Sn alloys have been previously reported [191], no evidence neither of these alloys nor of mixed oxides have been obtained by us, so the most suitable interpretation is that almost all the palladium dissolved in the third chemical step is inside the SnO<sub>2</sub>. This interpretation will also explain the Raman spectra modifications yet described.

#### **4.1.3.2. Addition of Pt using Sn(II) as reductor**

Figure 4.19 shows the XRD diffractograms of the sample containing the highest catalyst percentage ratio, which is practically the diffractogram obtained for the blank sample (i.e., that of polycrystalline SnO<sub>2</sub> [174]) with an additional phase attributed to the added catalyst. For all samples, the non-annealed (Figure 4.19a), the one annealed at 450 °C (Figure 4.19b) and the one annealed at 800 °C (Figure 4.19c), extra peaks corresponding to metallic polycrystalline platinum [186] are observed. Looking at the platinum peaks, it can be seen that, for both non-annealed or annealed at low temperatures samples, these peaks are wide, thus indicating that the procedure is good enough to form nanoclusters of metallic platinum at concentrations as high as nominal 10% atomic, greater than the usual concentrations used for gas-sensing applications. Moreover, these nanoclusters still remain at annealing temperatures as high as, at least, 450 °C, and only annealing at 800 °C makes the metallic platinum XRD peaks narrower, indicating the tendency to form greater clusters at high annealing temperatures, as is observed elsewhere [73]. The narrow peaks at annealing temperature of 800 °C are also observed for intermediate catalyst concentration (although the relative area of the peaks with respect to that of tin oxide is smaller). For the samples with nominal 0.2% atomic concentration of catalyst, no evidence of platinum phases is observed because the abundance of these phases lies below the XRD detection limit but the same behaviour would be expected, as will be discussed. The lattice parameters of the samples have been fitted and are summarised in table 4.17. No significant changes are observed.

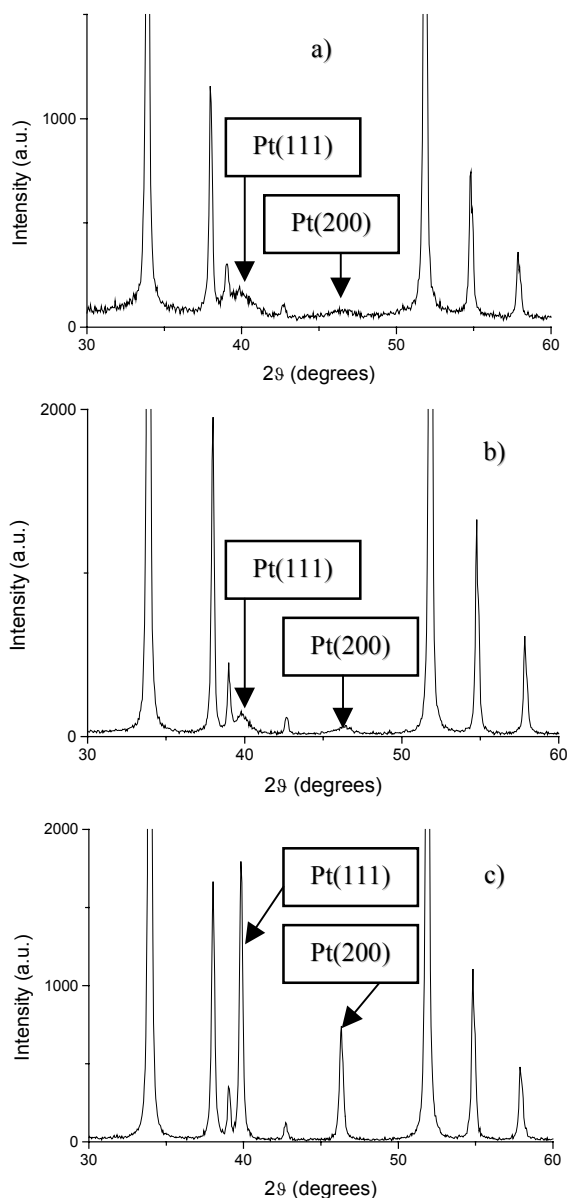


**Figure 4.19.** XRD diffractograms of 10% Pt, 10 SnSO<sub>4</sub>, a) non-annealed; b) annealed at 450 °C; c) annealed at 800 °C.

There are no noticeable differences among the different annealing temperatures applied (Figure 4.20a) nor within the different catalyst concentrations (Figure 4.20b), and only when comparing the complete set of results showed in table 4.18 with undoped samples, it can be appreciate that the Raman bands are displaced to slightly lower frequencies and are slightly wider than in the case of pure tin oxide. This confirms that the main oxidation state at all annealing temperatures corresponds to metallic platinum, because Raman would not detect metallic platinum due to its high reflectivity to the laser radiation used in these measurements, while the presence of any other platinum compound at sufficiently high concentration would have induced additional Raman bands and, although the Raman spectrum of PtO has not been previously reported, all the results presented along this work are in concordance with this conclusion. This is in contrast with the results obtained for palladium electroless addition, where the metallic state was

predominant at low annealing temperatures while PdO was primarily present at the appropriate high annealing temperature. Moreover, after annealing, palladium induced a displacement of the Raman bands that we attributed to the incorporation of palladium into the SnO<sub>2</sub> structure. This is not the case of platinum, allowing us to speculate that the incorporation of platinum into the SnO<sub>2</sub> structure is poor. This will be discussed again below.

Nominal Pt (at.%)	Reductor ratio (atomic)	Annealing T (°C)	a (Å)	c (Å)
0.2	1	-	4.737	3.186
0.2	10	-	4.737	3.187
2	1	-	4.737	3.186
2	10	-	4.737	3.186
10	1	-	4.737	3.186
10	10	-	4.737	3.186
0.2	1	200	4.736	3.185
0.2	10	200	4.735	3.185
2	1	200	4.737	3.186
2	10	200	4.736	3.186
10	1	200	4.737	3.186
10	10	200	4.736	3.185
0.2	1	450	4.735	3.185
0.2	10	450	4.736	3.186
2	1	450	4.736	3.186
2	10	450	4.735	3.185
10	1	450	4.735	3.185
10	10	450	4.736	3.185
0.2	1	800	4.736	3.186
0.2	10	800	4.736	3.186
2	1	800	4.736	3.186
2	10	800	4.735	3.185
10	1	800	4.735	3.185
10	10	800	4.735	3.185

**Table 4.17.** Cell parameters obtained after fitting the different XRD spectra.

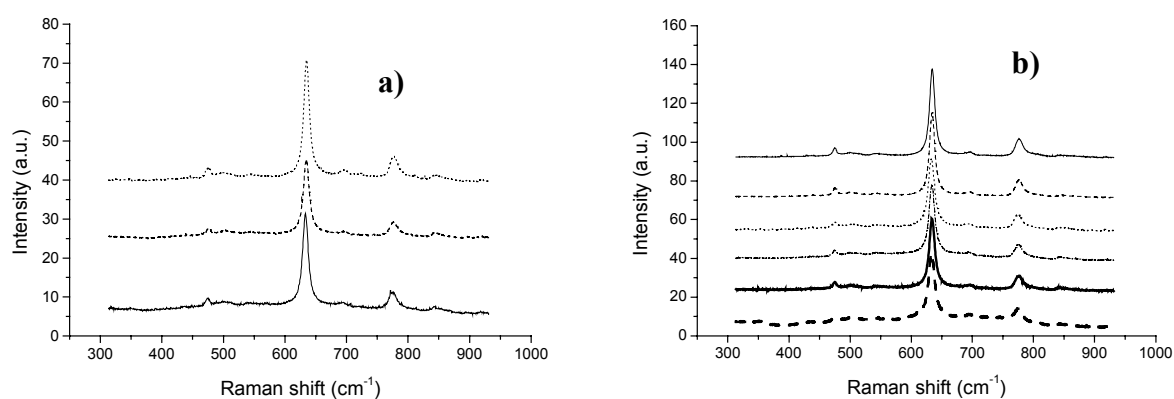


**Figure 4.20.** Raman spectra obtained from samples: a) — 10% Pt, non-annealed; ---- 10% Pt, annealed at 200 °C; ..... 10% Pt, annealed at 800 °C; b) Sample annealed at 450 °C, — 0.2% Pt, stoichiometric SnSO<sub>4</sub>; --- 0.2% Pt, 10 times more SnSO<sub>4</sub>; ..... 2% Pt, stoichiometric SnSO<sub>4</sub>; ---- 2% Pt, 10 times more SnSO<sub>4</sub>; — — 10% Pt, stoichiometric SnSO<sub>4</sub>; - - - 10% Pt, 10 times more SnSO<sub>4</sub>.

Additive conc. (atomic %)	Reductor Ratio	Annealing T (°C)	A <sub>1g</sub> Raman shift (cm <sup>-1</sup> )	A <sub>1g</sub> width (cm <sup>-1</sup> )
0.2	1	-	632.4	10.7
0.2	10	-	631.2	12.2
0.2	1	200	632.2	11.8
0.2	10	200	631.3	12
0.2	1	450	632.7	10.1
0.2	10	450	632.6	10.2
0.2	1	800	632.3	10.8
0.2	10	800	630.4	13.4
2	1	-	632.3	11.1
2	10	-	632.1	11.2
2	1	200	631.4	12.8
2	10	200	630.5	14.3
2	1	450	631.4	12.4
2	10	450	632.2	11.2
2	1	800	631.8	10.7
2	10	800	630.5	16.9
10	1	-	629.5	15.5
10	10	-	632.1	11.3
10	1	200	631.8	11.4
10	10	200	628.9	15.6
10	1	450	632.3	10.8
10	10	450	631.6	12
10	1	800	628.7	16.1
10	10	800	628.9	15.6

**Table 4.18.** Raman shifts and widths after fitting the Raman bands of the different spectra.

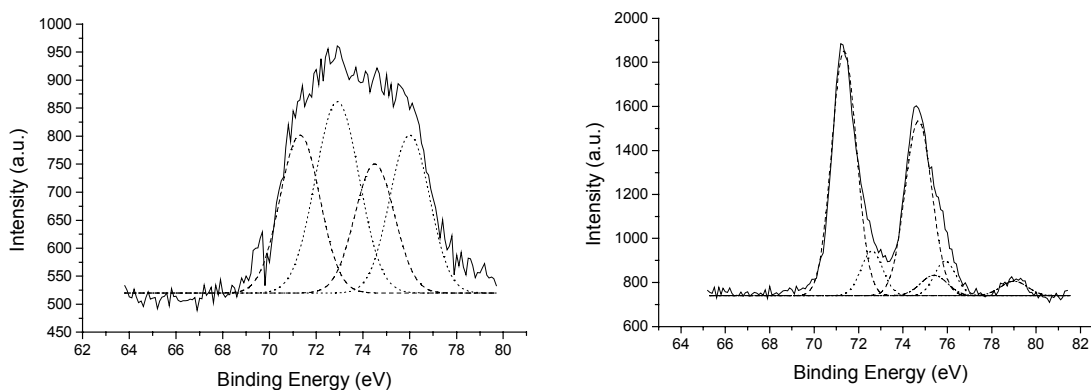


**Figure 4.21.** XPS spectra of the samples with 10% Pt, 10 SnSO<sub>4</sub>, a) Non annealed: — Acquired spectrum; --- Metallic Pt; ..... PtSO<sub>4</sub>; b) Annealed at 800 °C: — Acquired spectrum; --- Metallic Pt; ..... PtO; ---- PtO<sub>2</sub>.

Nominal Pt (at.%)	Reductor Ratio	Annealing T (°C)	S (at.%)	Pt (at.%)	Sn (at.%)	Pt/Sn (at.%)
0.2	1	-	3.7/ 0.6*	0.1/ 0.1*	20.5/ 39*	0.3/ 0.2*
0.2	10	-	4.4/ 1*	0.2/ 0.2*	19.7/ 40.6*	1.1/ 0.5*
0.2	1	200	3.5/ 0.4*	0.1/ 0.1*	24.5/ 39.9*	0.5/ 0.3*
0.2	10	200	4.2/ 0.8*	0.3/ 0.3*	22.5/ 36.3*	1.2/ 0.9*
0.2	1	450	0/ 0*	0.1/ 0.1*	30.1/ 39.1*	0.3/ 0.4*
0.2	10	450	0/ 0*	0.1/ 0.2*	27.7/ 36.5*	0.4/ 0.4*
0.2	1	800	0/ 0*	0/ 0*	29/ 40.8*	0/ 0*
0.2	10	800	0/ 0*	0.1/ 0.2*	28.5/ 39.7*	0.5/ 0.5*
2	1	-	4.1/ 0*	0.4/ 0.6*	20.1/ 38.1*	1.9/ 1.6*
2	10	-	5.1/ 1.6*	0.4/ 1.3*	20.1/ 39.8*	2.1/ 3.2*
2	1	200	3.7/ 0.3*	0.4/ 0.6*	22/ 39.1*	1.8/ 1.6*
2	10	200	5.1/ 1*	0.5/ 1.1*	20.1/ 39.1*	2.6/ 2.8*
2	1	450	0/ 0*	0.7/ 0.8*	29.1/ 36.8*	2.3/ 2.2*
2	10	450	0/ 0*	0.7/ 1*	24.6/ 37.6*	2.7/ 2.5*
2	1	800	0/ 0*	0.3/ 0.3*	28.8/ 40.6*	1/ 0.8*
2	10	800	0/ 0*	0.5/ 1.1*	30.2/ 39.9*	1.7/ 2.8*
10	1	-	4.2/ 1.9*	1.2/ 2.3*	20.8/ 37.8*	5.7/ 6.1*
10	10	-	5.6/ 1.9*	1.5/ 5.2*	16.6/ 36.6*	9/ 14.1*
10	1	200	4.9/ 2*	0.9/ 1.6*	22.4/ 40.3*	4/ 4*
10	10	200	5.9/ 2.4*	1.9/ 3.8*	19.2/ 31.2*	9.9/ 12.2*
10	1	450	-/ -*	1.1/ 1.4*	21.5/ 25*	5/ 5.5*
10	10	450	-/ -*	3.5/ 5.3*	19.9/ 34.5*	17.6/ 15.4*
10	1	800	0/ 0*	0.9/ 1.8*	29/ 40.8*	3.1/ 4.4*
10	10	800	0/ 0*	2/ 4.3*	31.1/ 39.8*	6.4/ 10.8*

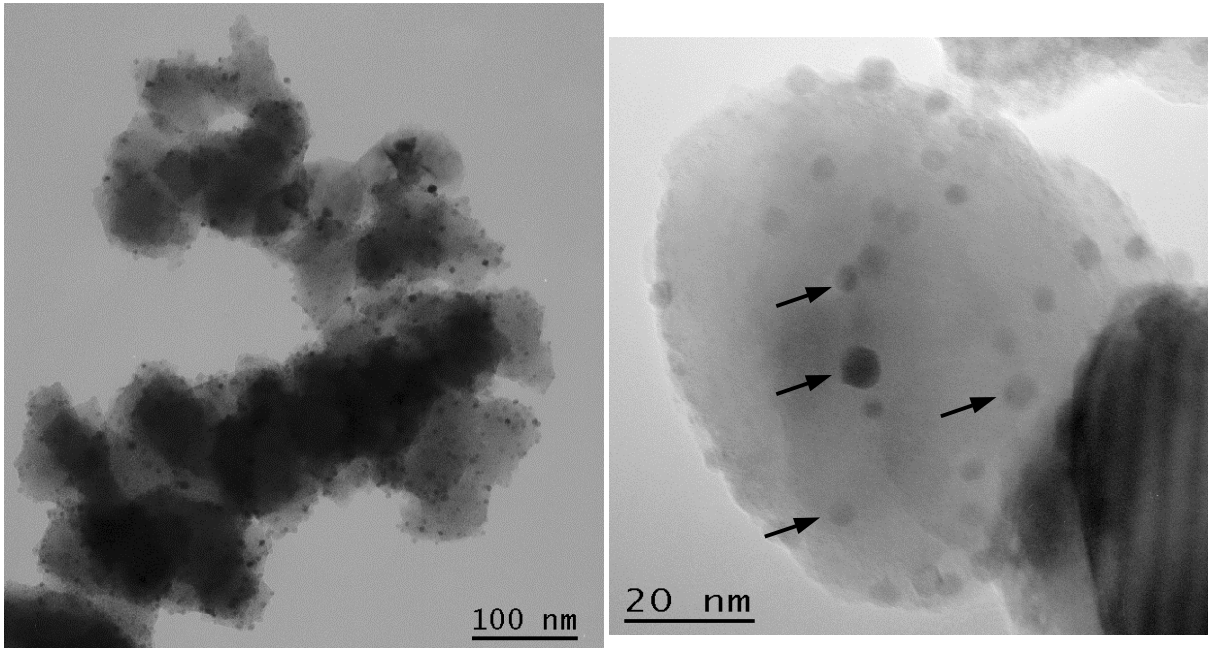
\*Values after sputtering.

**Table 4.19.** Atomic concentrations of the different elements on the samples obtained from the integration of the XPS spectra.

In order to know where the catalyst is distributed in the SnO<sub>2</sub> nanopowders, we have also investigated the XPS response of the differently prepared samples. The spectra of the sample with the highest catalyst concentration both non-annealed and annealed at 800 °C are shown in parts a and b of Figure 4.21, respectively. The fitting results verify the presence of metallic platinum (4f<sub>7/2</sub> peak at 71.2 eV) [192] and also of Pt(II) at all annealing temperatures. Pt(II) is mainly present as sulphate at low annealing temperatures and as PtO (4f<sub>7/2</sub> peak at 72.7 eV) [193] when annealing at 450 or 800 °C, where we also denote the presence of higher valence states of Platinum, Pt(IV) as PtO<sub>2</sub> (4f<sub>7/2</sub> peak at 75.0 eV) [194] on the surface. With respect to these fitting results, the fact that the areas of platinum(II) sulphate are similar to those of metallic platinum might be due to the fact that XPS is a surface analytical technique, thus indicating that in the surface there is a greater amount of sulphate than in the bulk. Nevertheless, metallic platinum is the primary at all annealing temperatures, since it is the only phase detected by XRD and HRTEM, and no platinum bands are detected in Raman. Moreover, the PtO present after annealing in air might probably come from the initial PtSO<sub>4</sub>, while PtO<sub>2</sub> might probably come from the disproportionation reaction of Pt(II). Atomic concentration results of the most significant elements obtained from the XPS spectra are summarised in table 4.19, where it can be seen that sulphur was completely eliminated only after annealing at 800 °C. It is again observed that the Pt/Sn ratio is sometimes higher than the nominal one, thereby suggesting that the catalyst is placed mainly on the tin oxide surface.

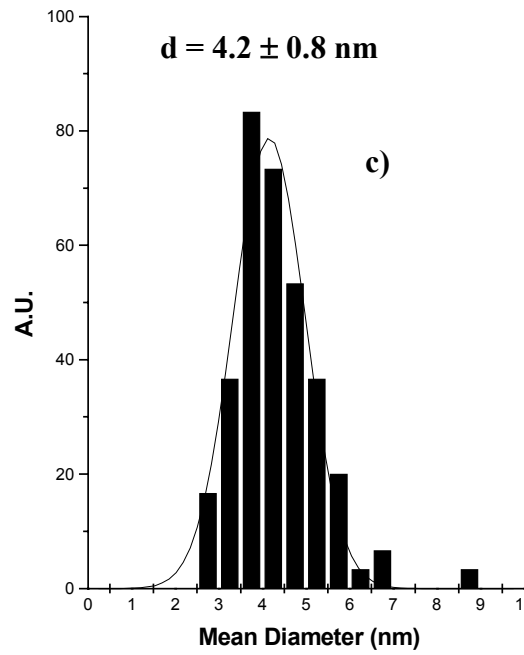
TEM analysis of the sample with highest catalyst concentration annealed at 450°C shows a homogeneous distribution of the Pt nanoclusters on SnO<sub>2</sub> nanoparticles (Figure 4.22). We calculated the mean nanocluster size from TEM micrographs and obtained that the mean diameter of the nanoclusters was 4.2 ± 0.8 nm (Figure 4.22c). These nanoclusters have also been analysed by means of HRTEM, and have been identified as metallic Pt, accordingly with the XPS and XRD results, and also confirming that Pt nucleates on the SnO<sub>2</sub> surface as metallic nanoclusters.

Figure 4.23.a) enlightens a Pt nanocluster placed on the surface of a SnO<sub>2</sub> nanoparticle of the sample showed in fig. 4.22. Lattice spacing of nanocluster was calculated on the Fast Fourier Transform of TEM micrograph. In this case, we obtained the spacing corresponding to the (111) Pt planes. We applied several frequency filters on the FFT image in order to separate those planes corresponding to Pt. The sample with highest catalyst concentration annealed at 800 °C (Figure 4.23b) also shows metallic Pt nanoclusters, although they are not homogeneously distributed on the SnO<sub>2</sub> nanoparticles surface, and moreover they appear in much lower quantity than when annealing at 450°C. These Pt nanoclusters are ranging in size between 2 and 5 nm. Notice that in this last case the (200) [interplanar distance 0.196 nm] platinum planes are parallel to the (110) [0.335 nm] SnO<sub>2</sub> plane [174,186]. Epitaxial growth structure of metal clusters formed on the oxide surface have been studied and communicated elsewhere [195-197].



a)

b)



**Figure 4.22.** a) TEM micrograph of the sample with nominal 10 atom % Pt, and a  $\text{SnSO}_4$  concentration of 10 times the stoichiometric ratio annealed at 450 °C. Pt nanoclusters appear in dark contrast on  $\text{SnO}_2$  nanopowders; b) Detail of fig. 4.22a.; c) Pt nanocluster size histogram of the sample showed in 4.22a.

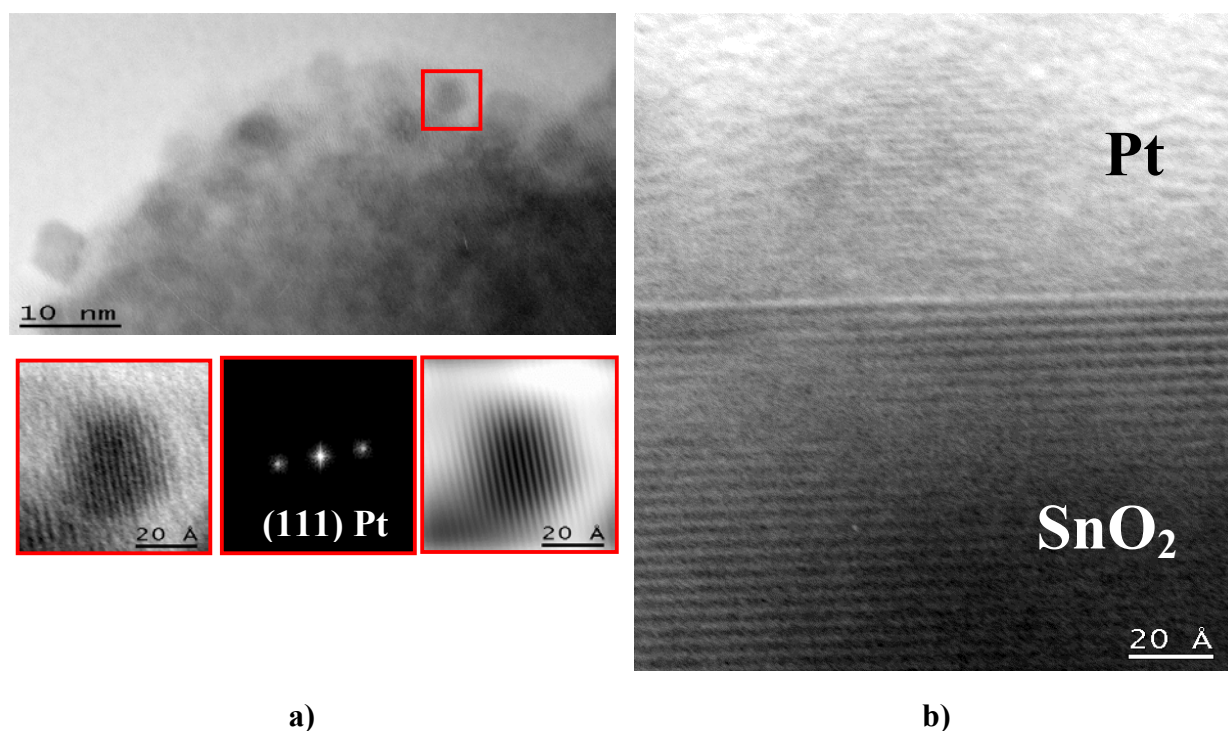


**Figure 4.23.** a) HRTEM micrograph of a metallic Pt nanocluster present on the sample with nominal 10 atom % Pt, and a SnSO<sub>4</sub> concentration of 10 times the stoichiometric ratio, annealed at 450 °C; b) HRTEM micrograph of a metallic Pt nanocluster present on the sample with nominal 10 atom % Pt, and a SnSO<sub>4</sub> concentration of 10 times the stoichiometric ratio, annealed at 800 °C.

Referring to the tin oxide valence band shape and the electronic states that configure it, there is an extensive bibliography describing the main features not only of the undoped tin oxide [174,198] but also informing about the platinum-induced surface states [83]. The valence band of samples with different catalyst concentrations annealed at 800 °C and 450 °C are shown in parts a and b of Figure 4.24 respectively. Surface states are located between the valence band and the Fermi level, behavior that coincides with data reported previously [35,57], and that must be associated with the influence of the catalyst. The density of surface states increases, of course, with catalyst concentration. Nevertheless, it must be stated that the shape of the valence band of our samples is clearly different from the data reported previously for Pt added by impregnation [35,57]. Thus, when dealing with electroless deposition, the density of population of surface states at 800 °C is similar throughout the entire range of binding energies from the top of the valence band until the Fermi level, indicating that our samples have a greater metal-like behaviour, which is in coincidence with the XRD, Raman and TEM data presented above. The shape of the valence band is also different when comparing the valence bands here reported with those reported for palladium obtained either by impregnation [57,124] or by electroless deposition. Nevertheless, it must be stated that, although the electroless addition of Pt gives valence bands of greater metal-like behavior, this does not mean that there is no structural interaction between Pt and SnO<sub>2</sub>. Thus, it is clear when comparing the valence bands showed in fig. 4.24a with the one reported for pure metallic Pt [199] that additional surface states are present in our case.

The fact that the valence band of the sample with highest catalyst percentage and annealed at 450 °C (Figure 4.24b) shows a high density of surface states around 3 eV is probably due to the greater amount of Sn(II) compounds coming from the reductor excess that are present in this sample. This is supported because the valence band of SnO has been reported to have a maximum density around 3 eV [176] and because, when looking at the other samples annealed at the same temperature (Figure 4.24b), all of them have a much lower density of surface states (even the one with the same nominal Pt concentration but where a stoichiometric concentration of reductor has been used). Moreover, HRTEM analysis of the sample with highest catalyst concentration annealed at 450 °C also reveals the presence of SnO.

The same shape of surface states is also observed in our samples at lower annealing temperatures, i.e., the valence band shape is similar to that of the sample with highest catalyst percentage and annealed at 450 °C (Figure 4.24b) when an excess reductor concentration is present, while in samples with stoichiometric reductor concentration, the valence band shape at all annealing temperatures is similar to that observed at 800 °C, thus confirming that the density of surface states associated with platinum is similar throughout the entire range of energies between the Fermi level and the SnO<sub>2</sub> valence band, and density differences of surface states of different energies arise mainly due to the presence of Sn(II) species.

When comparing the samples annealed at 450 °C and 800 °C, a greater interaction between Pt and SnO<sub>2</sub> is expected at 450 °C because, as has been previously discussed, at this temperature there is a greater amount of metallic Pt nanoclusters on the SnO<sub>2</sub> surface. Nevertheless, HRTEM images shown in fig. 3.23b also confirm that, even after annealing at 800 °C (where the mean cluster size of Pt increases), there are still some nanoclusters of Pt present on the SnO<sub>2</sub> surface and, moreover, preliminary gas sensor tests of these samples confirm that, for samples annealed at 450 or 800 °C, the gas sensor response with respect to pure tin oxide is improved, thereby confirming that there exists an interaction between the added Pt and the SnO<sub>2</sub> surface at all annealing temperatures.

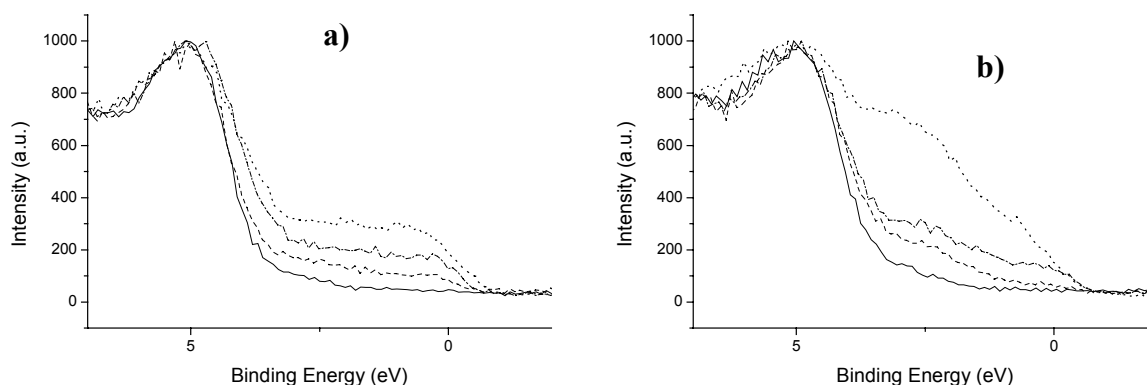


**Figure 4.24.** VB spectra for: a) samples annealed at 800 °C:- with a SnSO<sub>4</sub> concentration of 10 times the stoichiometric ratio: — , nominal 0.2 atom % Pt; --- , nominal 2 atom % Pt; ..... , nominal 10 atom % Pt ; - with a stoichiometric SnSO<sub>4</sub> concentration: - - - - , nominal 10 atom % Pt; b) samples annealed at 450 °C:- with a SnSO<sub>4</sub> concentration of 10 times the stoichiometric ratio: — , nominal 0.2 atom % Pt; --- , nominal 2 atom % Pt; ..... , nominal 10 atom % Pt ; - with a stoichiometric SnSO<sub>4</sub> concentration: - - - - , nominal 10 atom % Pt.

Nominal Pt/Sn (atomic%)	Nominal SnSO <sub>4</sub> /(NH <sub>4</sub> ) <sub>2</sub> PtCl <sub>4</sub>	Annealing T (°C)	Pt found/nominal Pt (%)	SnSO <sub>4</sub> (atomic%)	Pt inserted/total Pt (%)
0.2	1	-	18.4	8e-4	0
0.2	10	-	93.5	0.004	0
2	1	-	21.8	0.005	0
2	10	-	79	0.054	0
10	1	-	36.6	0.039	0
10	1	800	25.4	4e-4	3.6
10	10	-	90.5	0.139	0
10	10	800	60.7	8e-4	8.5

**Table 4.20.** Results obtained for the most significant samples after an ICP analysis.

Other differences are observed when comparing electroless with impregnation. With respect to the ICP results, they are summarised in Table 4.20. They show that the electroless method for the catalyst addition to the SnO<sub>2</sub> nanopowders is highly efficient, especially when using a higher reductor concentration. In this case, we find almost 90% of the expected Pt atomic concentration, although the amount of species aggregated from the reductor salt solution is also high. Thus, the efficiency, as obtained from our own results with impregnation in similar conditions (to our knowledge, no ICP results have been reported for Pt added samples), has a similar value than that of classical impregnation and much higher than that obtained in impregnation without evaporation to dryness. In the annealing process, the relative amount of platinum decreases both because some catalyst is lost and also due to the conversion of the reductor species to tin oxide because almost no reductor species are present after annealing. With respect to the results obtained for Pd electroless, the efficiencies are similar in both cases. Only a greater effect of the reductor concentration is observed in the case of platinum, as the efficiencies for the series with greater reductor concentration are higher than for Pd while with stoichiometric reductor concentration, they are lower. The ICP results showed that, in annealed samples, some platinum still dissolves after the third chemical step. One explanation may be the formation during annealing of species insoluble in aqua regia (as could be the case of some Sn-Pt alloys, that are reported elsewhere [200,201]), or the presence of platinum inside the SnO<sub>2</sub> nanopowders, that has also been observed in the case of Pd. When comparing with electroless-added palladium, the percentage of platinum dissolved after the third chemical step is much lower, thus confirming the discussion of the coincidence of these results with the Raman shifts observed. Nevertheless, further studies are needed to know which is the origin of this platinum, that only represents a maximum of a 8% of the added platinum.

#### **4.1.4. Addition of other metals**

##### **4.1.4.1. Addition of Ru using Sn(II)**

Figure 4.25 shows the XRD diffractograms of the sample containing the highest catalyst percentage ratio, which is practically the diffractogram obtained for the blank sample (i.e., that of polycrystalline SnO<sub>2</sub> [174]) with an additional phase attributed to RuO<sub>2</sub> [202] detected only after annealing at 800 °C. With respect to the calculated cell parameters, no changes can be observed, as summarised in table 4.21.

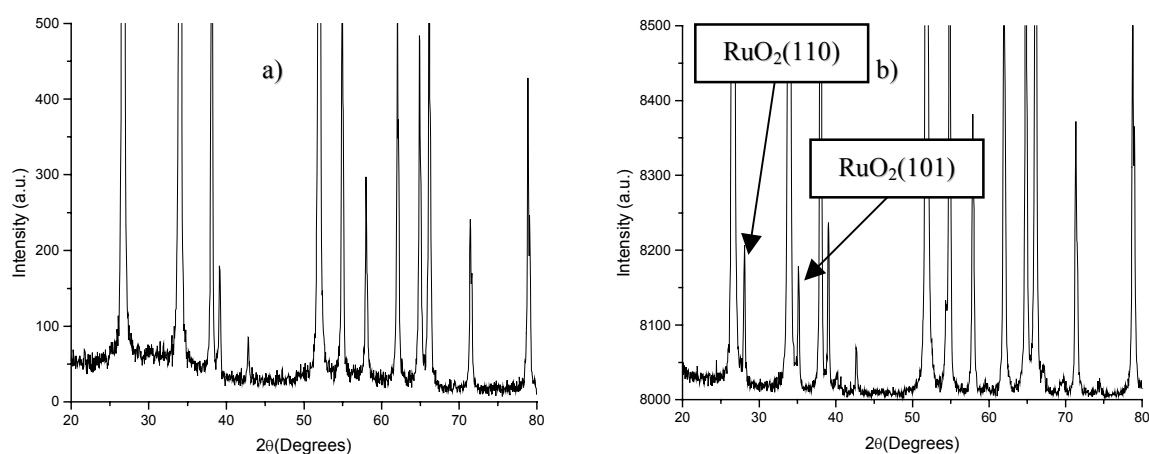


**Figure 4.25.** XRD diffractograms of a sample prepared from a solution of nominal 10 at.% Ru and SnCl<sub>2</sub> 10 times more concentrated than the stoichiometric quantity: a) non-annealed; b) annealed at 800 °C.

Nominal Ru (at.%)	Reductor ratio (atomic)	Annealing T ( °C)	a (Å)	c (Å)
0.2	1	-	4.736	3.186
0.2	10	-	4.735	3.185
2	1	-	4.736	3.185
2	10	-	4.735	3.185
10	1	-	4.736	3.185
10	10	-	4.736	3.185
0.2	1	450	4.736	3.186
0.2	10	450	4.737	3.187
2	1	450	4.736	3.186
2	10	450	4.737	3.186
10	1	450	4.737	3.187
10	10	450	4.735	3.185
0.2	1	800	4.736	3.186
0.2	10	800	4.735	3.185
2	1	800	4.736	3.186
2	10	800	4.736	3.186
10	1	800	4.734	3.185
10	10	800	4.735	3.186

**Table 4.21.** Summary of the cell parameters obtained after fitting the XRD spectra.

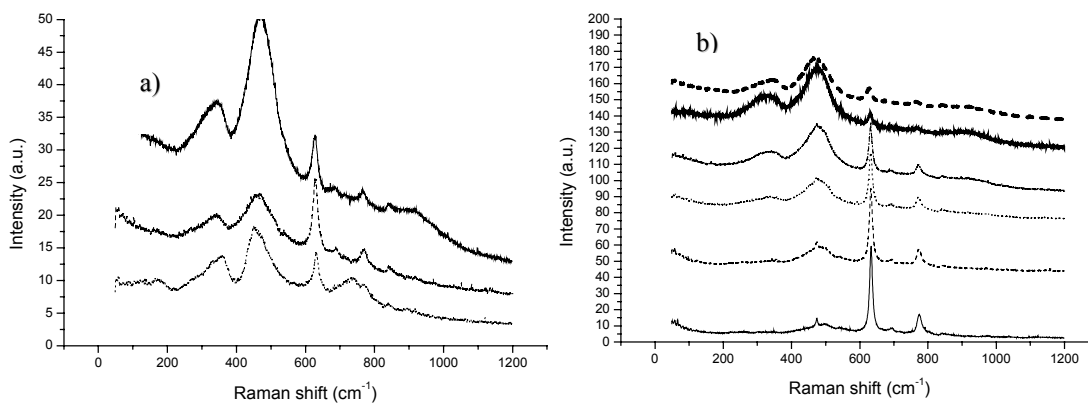


**Figure 4.26.** Raman spectra obtained from samples: a) nominal 10 atom % Ru, a concentration of  $\text{SnCl}_2$  10 times the stoichiometric ratio: —, non-annealed; ---, annealed at  $450^\circ\text{C}$ ; ·····, annealed at  $800^\circ\text{C}$ ; b) Samples without annealing: —, nominal 0.2 atom % Ru, stoichiometric  $\text{SnCl}_2$ ; ---, nominal 0.2 atom % Ru, and a concentration of  $\text{SnCl}_2$  10 times the stoichiometric ratio; ·····, nominal 2 atom % Ru, stoichiometric  $\text{SnCl}_2$ ; ·····, nominal 2 atom % Ru, and a concentration of  $\text{SnCl}_2$  10 times the stoichiometric ratio; — —, nominal 10 atom % Ru, stoichiometric  $\text{SnCl}_2$ ; — — —, nominal 10 atom % Ru, and a concentration of  $\text{SnCl}_2$  10 times the stoichiometric ratio.

Raman spectra of the whole set of samples are shown in fig. 4.26. It is clear from fig. 4.26.b) that ruthenium compounds are formed at room temperature, because additional bands (whose relative area with respect to  $\text{SnO}_2$   $A_{1g}$  peak increases with increasing Ru concentration) are detected. As the observed Raman bands do not coincide neither with chlorides nor with oxides reported in the bibliography [142], these bands must be associated with Ru-Sn compounds that have also been previously reported [172,203] and, as there are no reported values for the Raman spectra of these compounds, a fundamental study must be performed in order to associate each of these bands with a vibration of a certain compound. This study is beyond the scope of this work but, nevertheless, from fig. 4.26.a) it can be seen that there are changes in the present compounds as, for example, the Raman band at approximately  $900\text{ cm}^{-1}$  detected for non-annealed samples is not present after annealing, while an additional band at approximately  $750\text{ cm}^{-1}$  is present after annealing at  $800^\circ\text{C}$ . This behaviour can be due to the formation of Ru-Sn mixed oxides that, in certain conditions, have been shown to be the most stable phase after annealing [204,205]

With respect to the Raman  $\text{SnO}_2$   $A_{1g}$  peak, its behaviour with respect to the Ru concentration and the annealing temperature is reported in table 4.22. In general, the peak position shifts to lower values when the Ru concentration increases, while there is not a clear behaviour with respect to the annealing temperature applied. With respect to the width of the peak, it increases with the Ru concentration and does not change with the annealing temperature. These results might indicate that the Raman behaviour of the samples is dominated by the Ru-Sn compounds formed and, although these compounds have certain changes with the temperature, these changes do not alter very much the sample Raman features.

Additive conc. (atomic %)	Reductor Ratio	Annealing T (°C)	A <sub>1g</sub> Raman shift (cm <sup>-1</sup> )	A <sub>1g</sub> width (cm <sup>-1</sup> )
0.2	1	-	633.2	10.2
0.2	10	-	632.6	10.2
0.2	1	450	632.9	10.6
0.2	10	450	633.1	10.2
0.2	1	800	633	10.5
0.2	10	800	633.3	10.3
2	1	-	631.9	12
2	10	-	631.8	12
2	1	450	631.8	12.9
2	10	450	631.6	12.9
2	1	800	633.3	11.8
2	10	800	633.1	12.1
10	1	-	631	13.8
10	10	-	630.4	15.7
10	1	450	629.8	14
10	10	450	629.6	15.3
10	1	800	630.6	14.3
10	10	800	631.3	15.2

**Table 4.22.** Raman shifts and widths resulting from the fitting of the SnO<sub>2</sub> A<sub>1g</sub> Raman band.

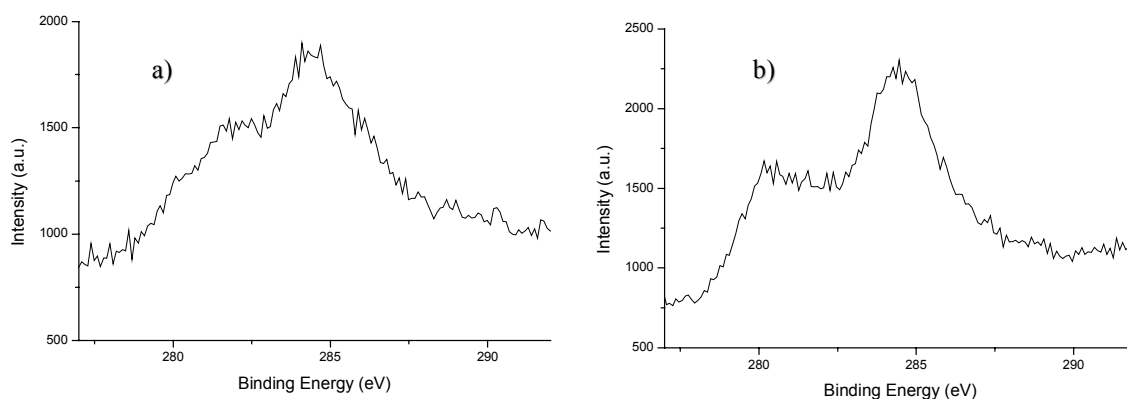


**Figure 4.27.** XPS spectra of samples obtained from a solution with nominal 10 atom % Ru and SnCl<sub>2</sub> 10 times more concentrated than the stoichiometric value: a) non-annealed; b) annealed at 800 °C.

In order to know where the catalyst is distributed in the SnO<sub>2</sub> nanopowders, we have also investigated the XPS response of the differently prepared samples. The spectra of the sample with the highest catalyst concentration both non-annealed and annealed at 800 °C are shown in parts a and b of Figure 4.27, respectively. With respect to the fitting results, only the detected atomic concentrations are discussed, since the presence of Ru-Sn compounds that have not been unambiguously characterised makes very difficult to analyse the Ru oxidation state, although from the spectra showed in fig. 4.27, it can be seen

that without annealing there is a greater amount of oxidised Ru than after annealing at 800 °C, and at both temperatures metallic Ru (3d<sub>5/2</sub> peak at 280.1 eV [149]) is present. Table 4.23 summarises the results of the concentration of elements calculated from XPS spectra, where it is again observed that chlorides are only eliminated after annealing at 800 °C.

Nominal Ru (at.%)	Reductor Ratio	Annealing T (°C)	Cl (at.%)	Ru (at.%)	Sn (at.%)	Ru/Sn (at.%)
2	10	-	4.8/ 2.5*	0.4/ 0.6*	27/ 38.6*	1.6/ 1.5*
2	10	450	2/ 1.1*	0.4/ 0.8*	25/ 34.3*	1.6/ 2.3*
2	10	800	0/ 0*	0.3/ 0.5*	29/ 37.7*	1/ 1.3*
10	10	-	10.2/ 6.2*	0.5/ 0.9*	26.6/ 35.5*	1.9/ 2.6*
10	10	450	3/ 1.6*	2.4/ 2.9*	18.7/ 25.3*	12.6/ 11.3*
10	10	800	0/ 0*	0.8/ 1.1*	27.8/ 34.4*	2.7/ 3.2*

\*Values after sputtering.

**Table 4.23.** Atomic concentration values of the most relevant elements obtained from XPS.

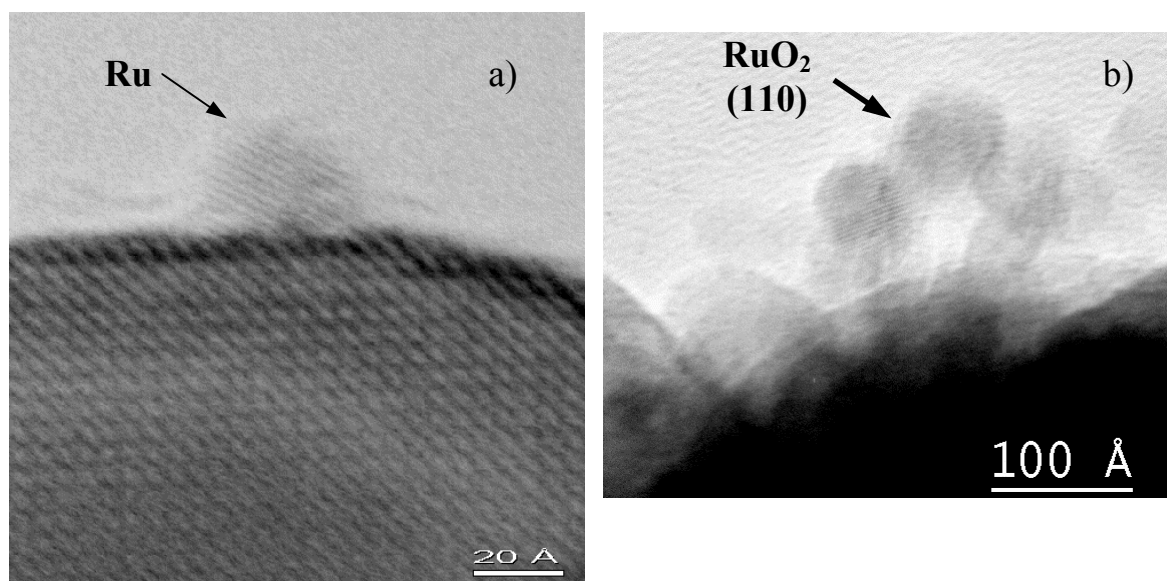


**Figure 4.28.** HRTEM images of the sample obtained from a solution with nominal 10 atom % Ru and SnCl<sub>2</sub> 10 times more concentrated than the stoichiometric: a) annealed at 800 °C; b) annealed at 450 °C. The identification has been done by means of CIS.

In HRTEM analysis, the sample with highest catalyst concentration was analysed both after annealing at 450 and 800 °C, and the results can be observed in fig. 4.28. Thus, as after annealing at 800 °C only some metallic Ru nanoclusters were detected, after annealing at 450 °C, a much greater amount of nanoclusters is detected, identified in this last case as RuO<sub>2</sub>.

Referring to the tin oxide valence band shape and the electronic states that configure it, the valence band of samples with different catalyst concentrations annealed at 800 °C is shown in the XPS response of Figure 4.29. Surface states are located between the valence band and the Fermi level, behavior that coincides with other additives, and that must be associated with the influence of the catalyst. The density of surface states increases, of course, with catalyst concentration but, in this case, the density difference is much lower than in other samples, thus indicating a lower interaction between the added catalyst and the tin oxide.

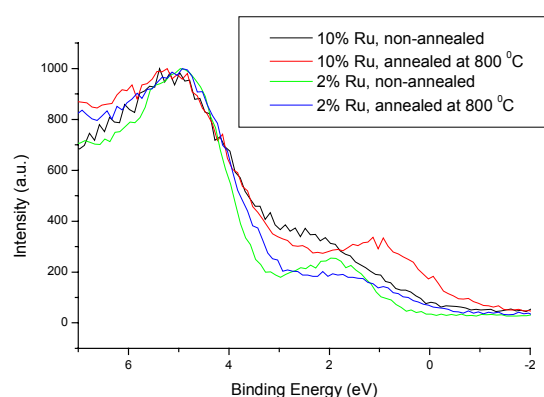


**Figure 4.29.** Valence band obtained from samples obtained from a solution with  $\text{SnCl}_2$  10 times more concentrated than the stoichiometric value and the nominal Ru concentrations and annealing temperatures indicated in the inset of the figure.

Nominal Ru/Sn (atomic%)	Nominal $\text{SnCl}_2/\text{K}_2\text{RuCl}_5$	Annealing T (°C)	Ru found/nominal Ru (%)	$\text{SnCl}_2$ (atomic%)	Ru acid/ total Ru (%)
2	10	450	56.9	-	-
2	10	800	51.8	-	-
10	1	-	15.3	4.2	88.8
10	1	450	13.1	-	-
10	1	800	13.1	-	-
10	10	-	38.7	21.7	97.7
10	10	450	38.3	-	-
10	10	800	36.1	-	-

**Table 4.24.** Summary of the concentrations obtained from ICP measurements.

The ICP results summarised in table 4.24 showed that, in this case, the efficiency of the addition method is not as high as electroless or impregnation to dryness. Nevertheless, the efficiency increases with increasing tin chloride concentration and decreases when annealing. The efficiency is higher at lower nominal Ru concentration. As in the case of electroless, tin chlorides are present on the surface of the sample in non-annealed samples, and at higher concentration when a greater excess of tin salt is present, but disappear after annealing. It can also be deduced that, in the non-annealed samples, almost all the ruthenium is dissolved in the first chemical step (that, in this case, is concentrated HCl), while after annealing all the Ru is dissolved in the alkaline fusion step. This is shocking, as metallic Ru is not soluble in HCl, and supports the fact, discussed in Raman spectra, that

the main part of the Ru is present as Ru-Sn compounds, that are different after annealing, because they are not longer soluble in acid.

#### 4.1.4.2. Addition of Ni using hypophosphide as reductor

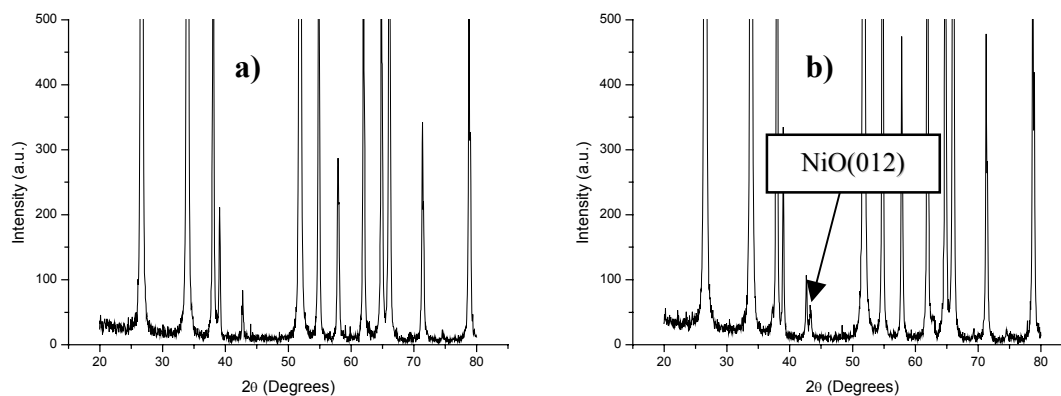


**Fig. 4.30.** XRD spectra of the sample with 10% nominal Ni and 10:1 reductor ratio: (a) non-annealed; (b) annealed at 800 °C.

The XRD results of the samples with highest additive concentration are shown in fig. 4.30. In the non-annealed samples, apart from the XRD peaks corresponding to polycrystalline SnO<sub>2</sub>, no additional peaks are observed. After annealing at 800 °C, the peaks corresponding to NiO [206] are present. The cell parameters of SnO<sub>2</sub> have been calculated for these samples and are presented in Table 4.25. No clear variation of the cell parameters is observed, neither with the additive concentration nor with the annealing temperature.

With respect to the Raman spectra, they are shown in figure 4.31. The results of the fitting of the SnO<sub>2</sub> A<sub>1g</sub> Raman band of these samples are summarised in table 4.26. From the Raman spectra, no additional bands to those of SnO<sub>2</sub> can be observed in non-annealed samples, while two additional Raman bands at around 500 and 540 cm<sup>-1</sup> are observed after annealing. These bands have a greater relative area with respect to the SnO<sub>2</sub> A<sub>1g</sub> Raman band when the Ni concentration increases and are attributed to NiO [207,208]. In general, it is observed from the data in table 4.26 that the SnO<sub>2</sub> A<sub>1g</sub> Raman band does not change in width, but its position is slightly shifted to lower values when increasing the catalyst concentration, while it slightly shifts to higher values when increasing the annealing temperature. With respect to the NiO bands, it is observed that their widths increase with the catalyst concentration, while they decrease with the annealing temperature. The Raman shift of the band at 500 cm<sup>-1</sup> shifts to higher values when increasing the catalyst concentration. All these features might be due to structure interactions between the catalyst and tin oxide, as will be discussed below.

Nominal Ni (at.%)	Reductor ratio (atomic)	Annealing T ( °C)	a (Å)	c (Å)
0.2	1	-	4.736	3.185
0.2	10	-	4.736	3.186
2	1	-	4.737	3.186
2	10	-	4.736	3.186
10	1	-	4.736	3.185
10	10	-	4.737	3.186
0.2	1	450	4.737	3.186
0.2	10	450	4.738	3.187
2	1	450	4.736	3.185
2	10	450	4.735	3.185
10	1	450	4.735	3.185
10	10	450	4.738	3.187
0.2	1	800	4.737	3.186
0.2	10	800	4.737	3.186
2	1	800	4.736	3.185
2	10	800	4.736	3.186
10	1	800	4.735	3.185
10	10	800	4.736	3.185

**Table 4.25.** Cell parameters calculated from the fitting of XRD spectra.

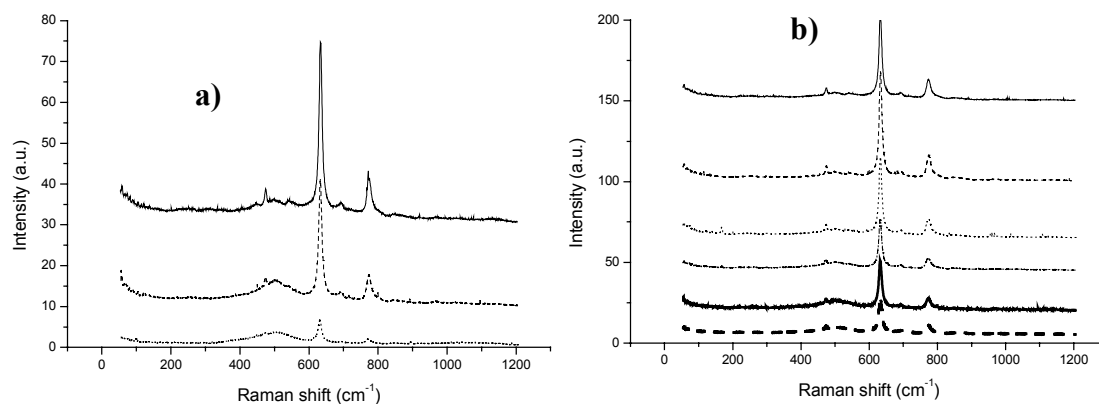


**Fig. 4.31.** Raman spectra obtained from samples: a) nominal 10 atom % Ni, a concentration of  $\text{Na}_2\text{HPO}_2$  10 times the stoichiometric ratio: — , non-annealed; ---- , annealed at 450 °C; ······ , annealed at 800 °C; b) Samples annealed at 450 °C: — , nominal 0.2 atom % Ni, stoichiometric  $\text{Na}_2\text{HPO}_2$ ; --- , nominal 0.2 atom % Ni, and a concentration  $\text{Na}_2\text{HPO}_2$  of 10 times the stoichiometric ratio; ······ , nominal 2 atom % Ni, stoichiometric  $\text{Na}_2\text{HPO}_2$ ; ---- , nominal 2 atom % Ni, and a concentration of  $\text{Na}_2\text{HPO}_2$  10 times the stoichiometric ratio; ——— , nominal 10 atom % Ni, stoichiometric  $\text{Na}_2\text{HPO}_2$ ; — — , nominal 10 atom % Ni, and a concentration of  $\text{Na}_2\text{HPO}_2$  10 times the stoichiometric ratio.

Additive conc. (atomic %)	Reductor Ratio	Annealing T (°C)	A <sub>1g</sub> Raman shift (cm <sup>-1</sup> )	A <sub>1g</sub> width (cm <sup>-1</sup> )	NiO Raman shift (cm <sup>-1</sup> )	NiO Width (cm <sup>-1</sup> )	NiO/A <sub>1g</sub> Relative area(%)	NiO Raman shift (cm <sup>-1</sup> )	NiO width (cm <sup>-1</sup> )	NiO/A <sub>1g</sub> relative area(%)
0.2	1	-	633.1	10.3	-	-	-	-	-	-
0.2	10	-	633.4	10.7	-	-	-	-	-	-
0.2	1	450	633.2	10.1	-	-	-	-	-	-
0.2	10	450	633.5	10.1	-	-	-	-	-	-
0.2	1	800	633.4	10.1	-	-	-	-	-	-
0.2	10	800	633.6	10	-	-	-	-	-	-
2	1	-	632.6	10.4	-	-	-	-	-	-
2	10	-	632.5	10.5	-	-	-	-	-	-
2	1	450	633	10.4	500.1	39.8	17	542.4	18.4	3.9
2	10	450	632.5	10.8	500.8	51.6	39.1	541.9	23.9	7.4
2	1	800	633.3	10.1	500.2	31.5	10.3	542.7	15.1	2.9
2	10	800	633.5	10.3	500.6	35.2	12.2	542	16.1	3.2
10	1	-	632.5	10.2	-	-	-	-	-	-
10	10	-	632.1	10	-	-	-	-	-	-
10	1	450	632.7	10.8	504.4	55.6	52.3	542.7	27.2	9
10	10	450	632.5	10.8	505.5	68	65.3	542.2	30	6.3
10	1	800	633.3	10.4	506.5	43.4	125.9	541.5	20.1	17.5
10	10	800	633.6	10.1	503.7	62.9	129.8	543.5	22.1	14.2

**Table 4.26.** Summary of the fitting of the most relevant features of the Raman spectra.

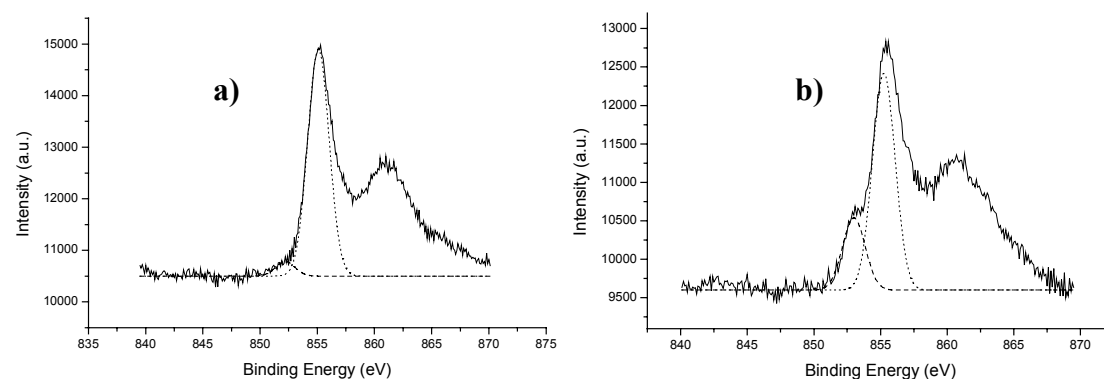


**Figure 4.32.** XPS spectra of the samples obtained from solutions with nominal 10% Ni and a concentration of Na<sub>2</sub>HPO<sub>2</sub> 10 times the stoichiometric ratio: a) non annealed: — Acquired spectrum, --- Metallic nickel, ..... NiO; b) annealed at 800 °C: — Acquired spectrum, --- Metallic nickel, ..... NiO.

The XPS characterisation of these samples is presented in fig. 4.32 and the atomic concentration results of the XPS spectra fitting are summarised in table 4.27, where it is observed that Ni/Sn ratio is always higher before sputtering, thus indicating that the catalyst is mainly present on the surface of the SnO<sub>2</sub> nanoparticles. It can also be seen that P is not eliminated even after annealing at 800 °C. The valence band spectra obtained for these samples is shown in fig. 4.33. With respect to the fitting of the oxidation states, it must be stated that the fitting hereby presented is only qualitative, since the presence of NiO is detected at all annealing temperatures and the analysis of the XPS spectrum of NiO and the possible presence of Ni<sub>2</sub>O<sub>3</sub> is still nowadays a subject of investigations because of the features that it presents [209-211]. Thereby, we have identified metallic Ni and NiO (2p<sub>3/2</sub> peaks at 852.7 and 853.8 eV respectively [149]) at all temperatures, with a higher amount of metallic Ni after annealing at 800 °C. This behaviour is also confirmed looking

at the valence bands presented, where there are surface states associated with the catalyst and there is a higher density of these states near the Fermi level in samples annealed at 800 °C, thus indicating a greater metal-like behaviour of these samples.

Nominal Ni (at.%)	Reductor Ratio	Annealing T (°C)	P (at.%)	Ni (at.%)	Sn (at.%)	Ni/Sn (at.%)
2	10	-	0.5/ 0.4*	3.6/ 1.7*	24/ 39.8*	15/ 4.3*
2	10	450	0.6/ 0.3*	2.9/ 1.7*	23.6/ 38.1*	12.1/ 4.4*
2	10	800	0.8/ 0.4*	2.4/ 1.4*	24.4/ 39.2*	9.9/ 3.6*
10	10	-	1.9/ 0.8*	3.1/ 1.9*	20.9/ 37.6*	15/ 5.1*
10	10	450	1.6/ 0.4*	3.7/ 2.8*	21/ 36*	17.5/ 7.6*
10	10	800	2.7/ 1.3*	3/ 2.4*	19.4/ 34.7*	15.3/ 6.9*

\*Values after sputtering.

**Table 4.27.** Atomic concentration results of the most relevant elements obtained from the fitting of XPS spectra.

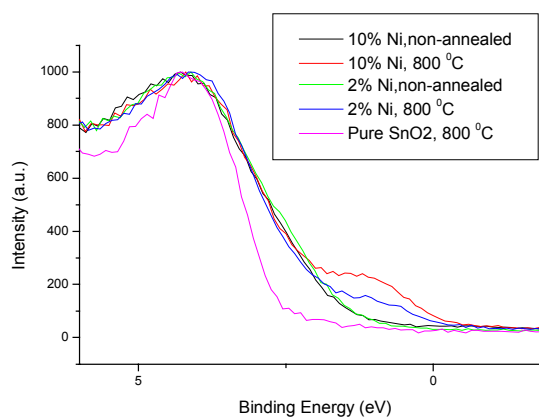


**Figure 4.33.** Valence band acquired from samples obtained from a solution with  $\text{Na}_2\text{HPO}_2$  10 times more concentrated than the stoichiometric value and the nominal Ni concentrations and annealing temperatures indicated in the inset of the figure.

The TEM results of these samples show structures like the one observed in fig. 4.34. It is observed that Ni forms sticks of NiO on the  $\text{SnO}_2$  surface, both after annealing at 450 or at 800 °C. This must be due either to the kind of interaction between NiO and  $\text{SnO}_2$  or to the mechanism of addition using hypophosphide as reductor, as in this case the process begins with the adsorption of the reductor on the substrate surface, followed by the reduction of the metal on this adsorbed reductor.

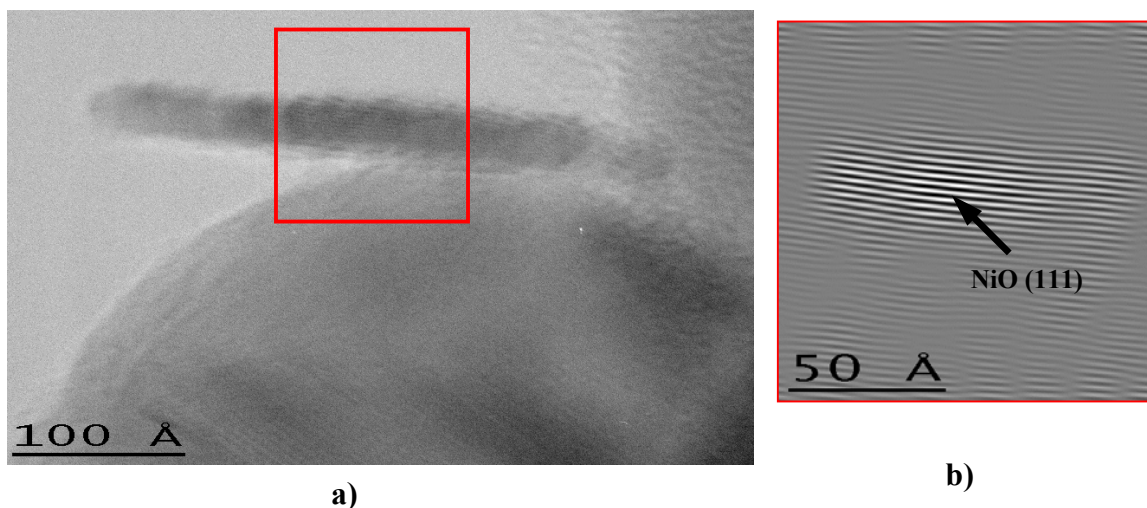


**Fig. 4.34.** a) TEM image of the typical Ni features observed after annealing either at 450 or at 800 °C. In this case, the image has been taken on a sample obtained from a solution containing 10 atom % Ni and a concentration of  $\text{Na}_2\text{HPO}_2$  10 times greater than the stoichiometric value, after annealing at 800 °C. b) HRTEM image of the Ni stick. CIS has been applied to this image to identify it as NiO.

The ICP results shown in table 4.28 state that the efficiency of nickel addition to  $\text{SnO}_2$  is very high at all annealing temperatures, although is a little less after annealing. As discussed with the other electroless results presented, the efficiency increases when a higher ratio of reductor is used, although in this case this is only observed previous to annealing, and the difference is low. Moreover, the ICP results show the presence of nickel into  $\text{SnO}_2$  after annealing at 450 °C. It must be stated that, in the samples annealed at 800 °C, there was a portion of  $\text{SnO}_2$  very difficult to solubilize, probably because of some chemical interaction between the reductor and the substrate, as observed in other substrates [212-214]. This interaction has diffculted the detection of Ni inserted and, thereby, we have not included any value in these positions.

Nominal Ni/Sn (atomic%)	Nominal $\text{Na}_2\text{HPO}_2/\text{NiCl}_2$	Annealing T (°C)	Ni found/nominal Ni (%)	Ni inserted/total Ni (%)
2	10	450	94	20.9
2	10	800	90	?
10	1	-	88.7	0
10	1	450	83.9	16.6
10	1	800	79.2	?
10	10	-	95.4	0
10	10	450	73.7	28.6
10	10	800	61	?

**Table 4.28.** Summary of the concentration Ni found by means of ICP analysis in the most relevant samples.

## 4.2. Applications

Until now, we have described the main characteristics of different methods of catalyst addition to SnO<sub>2</sub>. Although it is not the main aim of this work, it is also important to have a general view of the possible applications of the developed process for the improvement of existing gas sensors. This is briefly done in this section, where results of catalytic conversion of CO to CO<sub>2</sub> from FTIR measurements are reported for different samples.

### 4.2.1. Catalytic conversion of CO

The catalytic conversion of CO to CO<sub>2</sub> was measured for different samples by means of FTIR. Thus, a “home-made” film of the desired powder was formed on an alumina substrate. The sample was then introduced in a sealed chamber provided with a heater to control the temperature, and a flux of 20 ml/min of 1000 ppm of CO in synthetic air was applied. Afterwards, the area of the CO<sub>2</sub> peak was measured with a FTIR spectroscope. The measures were acquired with 50 acquisitions and a pass of 0.2, with an initial equilibration time of 90 minutes in order to have a stationary CO<sub>2</sub> concentration at room temperature. This concentration was measured as background signal and was subtracted from the areas of the CO<sub>2</sub> IR peaks measured at higher temperatures. An equilibration time of 30 minutes was enough to reach the equilibrium when the temperature was changed.

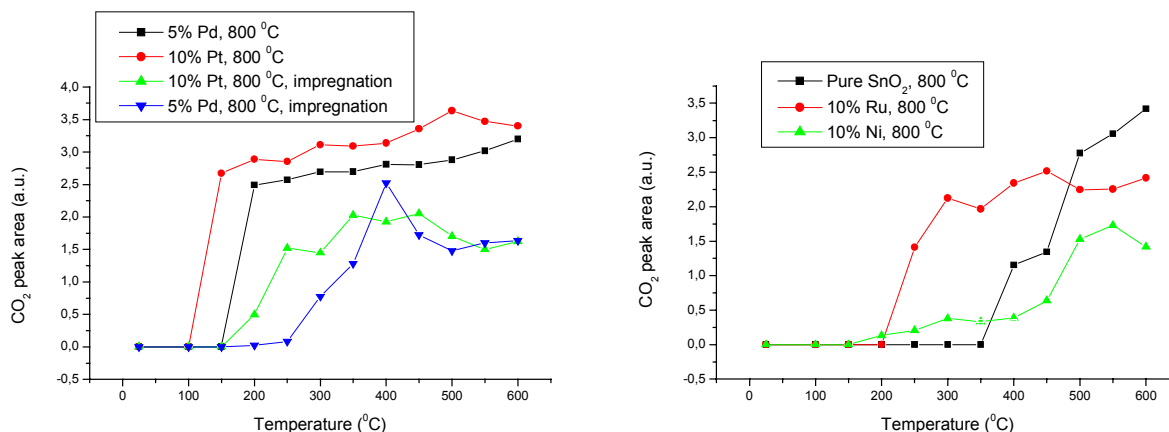


**Figure 4.35.** Variation with respect to the temperature of the area of the FTIR CO<sub>2</sub> peak subtracted from the one at room temperature for different samples. In all cases, the metal concentrations indicate the nominal value while a concentration of reductor 10 times greater than the stoichiometric value was used. The samples labeled with ‘impregnation’ are those obtained adding the metal by means of impregnation to dryness.

The obtained results for different additives and addition methods are presented in fig.4.35. Together with these results, obtained with dry ambient, the same study was performed for a couple of additives in an ambient saturated of humidity to study if there is any influence of the water in this process. The results are presented in fig.4.36.

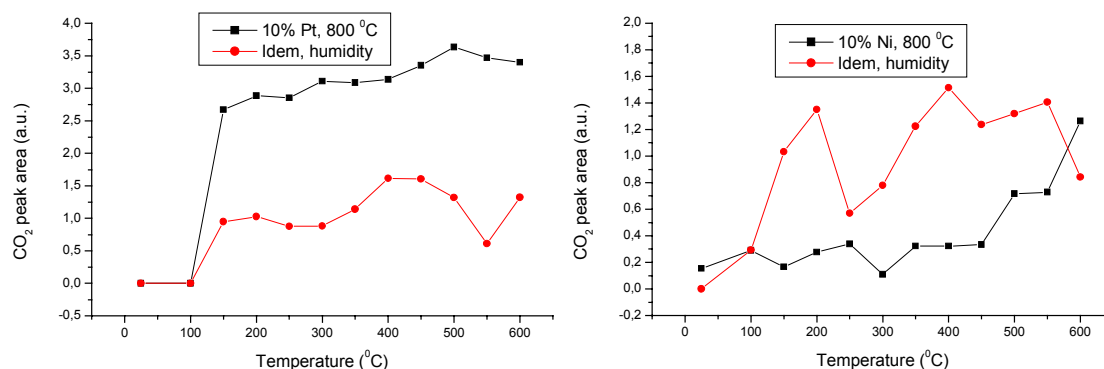


**Figure 4.36.** Variation with respect to the temperature of the area of the FTIR CO<sub>2</sub> peak subtracted from the one at room temperature for different samples. In all cases, the metal concentrations indicate the nominal value while a concentration of reductor 10 times greater than the stoichiometric value was used. The samples labeled with ‘humidity’ are those obtained measuring with a gas ambient saturated with humidity.

When discussing the presented results, only a comparison between the different studied samples can be done, because of the experimental errors of the measures:

- the film obtention method is not completely reproducible,
- the reported temperature is the one programmed, that is always higher than the real one, and the difference between both temperatures increases at higher temperatures,
- the concentrations are not reproducible, since the gas flux is only manually controlled. Moreover, the test chamber is not completely sealed.

Nevertheless, all these experimental errors, at least those concerning the control of temperature, can be considered as systematic, i.e., the measured temperature can be considered to be approximately the same for all the samples, although the real temperature value is lower than the one here presented. Thereby, the results show that the metal addition promotes the catalytic conversion of CO, as the temperature where the conversion begins of pure SnO<sub>2</sub> is the highest. Moreover, the initial conversion temperatures decrease in the order: Ru>Pd impregnated>Pt impregnated>Pd electroless>Pt electroless, and only Ni shows a strange behaviour, that can be due to the fact that there is some amount of CO conversion at room temperature (remember that, to obtain the CO conversion, we are subtracting the response obtained at room temperature). It can be also observed that the presence of water does not influence the temperature of initial CO conversion, at least in the case of Pt and Ni.

### 4.3. Discussion

Two general features arise when looking at the results presented in this section of the work: 1) the addition method influences the additive deposition and 2) each additive behavior depends on its intrinsic properties but also on its specific interaction with the substrate. Both of them are widely known, so in this work we have only stated them once again.

In general, we have seen that the impregnation method, when used in one step and until evaporation to dryness, gives big clusters of the initially solubilized metal salt, without changing the oxidation state of the metal. This is not surprising, since it is just a recrystallization procedure where the metal salt is solubilized and recrystallizes again when evaporating the solvent because of precipitation due to the achievement of supersaturated solutions. This is the classical addition process of metals on tin oxide but, as stated above, it has different drawbacks: first of all, a certain degree of evaporation of the solvent is needed in order to promote nucleation processes of the dissolved ions that can give clusters added to the support. If there is no evaporation, there is a few amount of metal added but, if the evaporation is complete, the formed clusters are very big if the metal salt concentration in the solution is high. Thereby, in order to obtain high metal concentrations with low cluster sizes, the only way is to perform several impregnation steps with partial evaporation of the solvent each time. Since this is a trial-and-error method, it is quite complicated to perform. Nevertheless, since usual concentrations of metals for gas-sensing materials are quite low, the classical process can be good enough because the metal salt concentration in solution can be low, thereby difficulting the growth of the nuclei formed during the supersaturation process.

On the other hand, the rest of the processes studied in this work imply chemical (in the case of Ru) or electrochemical reactions (for Pd, Pt and Ni). Thus, in the case of Ru, the formation of compounds with Ru-Sn bonds gives a certain quantity of precipitated nanoclusters of these compounds added on the support surface. In the other cases, an electrochemical reaction takes place, giving metallic nanoclusters on the support surface. In all the cases, few big clusters of the metal are formed in non-annealed samples because of the different mechanisms involved in the addition process with respect to impregnation.

The above described processes take place at room temperature (or, in the case of impregnation, at temperatures lower than the boiling point of water, that is the most used solvent). Nevertheless, as the material must be stabilized in order to have a good gas-sensing device, an annealing process must be performed. This process must be made in the 'blank' atmosphere that will be used afterwards and, for the aim of this work, this means that the annealing must be performed in air. Moreover, the annealing temperature must be higher than the highest temperature at which the device will be used. In our case, this means that 450 °C is enough, since usual operating temperatures for the detection of CO or methane (that are the gases here investigated) are lower.

When annealing the samples, the metals present behave depending on their initial oxidation state, their intrinsic chemical properties and on their specific interaction with the substrate. Thereby, the different metals studied in this work behave as follows:

- Pd tends to oxidize when annealed in air. Thereby, both the PdCl<sub>2</sub> or the metal present in non-annealed samples oxidize to PdO and PdO<sub>2</sub>. The interaction of

palladium with SnO<sub>2</sub> gives rise to two phenomena from the chemical point of view: the stabilization of PdO<sub>2</sub> and also the insertion of a great amount of palladium into SnO<sub>2</sub>. From the electronic point of view, the palladium present on the SnO<sub>2</sub> surface creates surface states located in the semiconductor 'gap'. This is a common feature of all the added metals, and it is precisely what is searched, since these surface states are the responsible for the improved characteristics of the material with respect to pure tin oxide. The created surface states will depend on the metal added and its chemical and crystallographic state, thereby giving rise to the different gas-sensing responses observed for different metals but also for different addition methods.

- Pt does not oxidize if it is initially present in metallic state, but it does form PtO when Pt(II) salts are present in non-annealed samples. Moreover, the initial Pt(II) also disproportionates to metallic Pt and PtO<sub>2</sub>. The interaction of platinum with SnO<sub>2</sub> promotes the fact that, when annealed at sufficiently high temperature, platinum tends to form big metallic clusters independently of its initial state, and it does not insert greatly into the substrate. Nevertheless, the minimum temperature of formation of the big metallic platinum clusters can be changed, as can be observed when comparing the XRD spectra of the samples added by impregnation and electroless and annealed at 450 °C.
- Ru is initially present forming nanoclusters of compounds with Ru-Sn bonds. When annealing in air, the ternary system Ru-Sn-O (where the substrate also influences) gives rise to different compounds that, at high temperatures and Ru loadings, also give a certain amount of metallic Ru and RuO<sub>2</sub> nanoclusters.
- Ni is probably present in metallic state just after the electroless process, but it is oxidized even at room temperature. An annealing temperature of 450 °C is enough to form NiO, and the interaction of nickel with SnO<sub>2</sub> promotes the fact that, when annealing, NiO is present as sticks rather than as nanoclusters on the SnO<sub>2</sub> surface, and nickel does insert (at least to a certain amount) into the substrate.

As it has been mentioned above, certain additives, as Pd, seem to be inserted into SnO<sub>2</sub>. This fact must be discussed with caution as, in general, what is labeled throughout this work as 'metal inserted' is the amount of metal that is not dissolved in the first chemical step of dissolution that has been developed in order to do the ICP analysis of the samples. Thus, in the case of Pd, the insertion of the metal into the SnO<sub>2</sub> seems to be the most suitable explanation, as it is majoritary and no Pd-Sn or other kind of compounds are detected. Nevertheless, as discussed above, in the case of Pt this 'insertion' is minority and can be an artifact due to the presence of Pt-Sn or other kind of compounds not soluble in aqua regia. The same care must be applied for the results presented in the case of Ru (where, in fact, we have no information about the quantity of metal inserted, if there is any) and Ni. Moreover, throughout this work, it has been stated that the SnO<sub>2</sub> cell parameters calculated from the XRD spectra do not seem to change in any case. This fact can, in principle, be considered as contradictory to the insertion as, if a great amount of metal is inserted into the SnO<sub>2</sub>, some change in the SnO<sub>2</sub> cell parameters must be expected. Nevertheless, two facts must be considered: first of all, the real metal concentrations present in the samples are, in the best of the cases, not much higher than the XRD detection limit and, secondarily, as the metals are added on stabilized SnO<sub>2</sub> (i.e., an SnO<sub>2</sub>

whose crystalline structure is completely formed and does not change very much with the annealing temperature), if insertion takes place, it must be expected to take place only in the first superficial layers of the SnO<sub>2</sub> and not on the whole bulk of the SnO<sub>2</sub> nanocrystals. As the cell parameters are calculated for the bulk of the sample, the variation of the cell parameters produced on few surface layers might not be detected.

With respect to the annealing process, as above mentioned, the temperature must be high enough to stabilize the material but the finally used temperature can change. Thus, for example, in the case of platinum, if we are trying to use it to increase the sensitivity of the material to CO, it should be in metallic state and in form of nanoclusters on the SnO<sub>2</sub> surface. Thus, in the case of samples added by electroless, an annealing temperature of 450 °C is enough, since the temperature is high enough to stabilize the material and, at this temperature we have metallic nanoclusters on the SnO<sub>2</sub> surface, and if the temperature is high enough, the nanoclusters are no longer present. Nevertheless, when platinum is added by impregnation, the samples annealed at 450 °C does not have metallic nanoclusters. In fact, when adding Pt by impregnation on TiO<sub>2</sub>, it has been seen that Pt forms big metallic clusters when annealing at 450 °C and the detection of some Pt nanoparticles on the TiO<sub>2</sub> surface is only possible after annealing at 800 °C because of the separation of some particles from the big Pt clusters.

Thus, the final material will have a different gas-sensing behavior depending on the metal added and on the chemical and crystallographic state of the additive, i.e., depending on the addition method. This is clearly shown in the application here tested. For example, in the case of CO catalytic conversion, it is evident that the addition of a metal lowers the initial conversion temperature, and this temperature depends not only on the metal added (for example, it is observed that electroless Pt gives the lowest temperature) but also on the addition method used as, for example, initial catalytic conversion temperatures are lower when using electroless addition than when using impregnation.